AGU PUBLICATIONS

JGR

Journal of Geophysical Research: Atmospheres

RESEARCH ARTICLE
10.1002/2017JD026576

Key Points:
- Superparameterization and CLUBB improve CAM5 rain rate and diurnal cycle in Amazonian wet season
- Superparameterization realistically captures the relationships between environmental conditions and rainfall
- Improved lower tropospheric moisture, shallow-to-deep transition, and cloud microphysics with aerosol effect are likely responsible

Correspondence to:
K. Zhang,
kzkaizhang@utexas.edu

Citation:
Zhang, K., Fu, R., Shaikh, M. J., Ghan, S., Wang, M., Leung, L. R., … Marengo, J. (2017). Influence of superparameterization and a higher-order turbulence closure on rainfall bias over Amazonia in Community Atmosphere Model version 5. *Journal of Geophysical Research: Atmospheres*, *122*, 9879–9902, https://doi.org/10.1002/2017JD026576

Received 31 JAN 2017
Accepted 24 AUG 2017
Accepted article online 29 AUG 2017
Published online 21 SEP 2017

Influence of Superparameterization and a Higher-Order Turbulence Closure on Rainfall Bias Over Amazonia in Community Atmosphere Model Version 5

Kai Zhang[1], Rong Fu[1,2], Muhammad J. Shaikh[1], Steven Ghan[3], Minghuai Wang[4,5], L. Ruby Leung[3], Robert E. Dickinson[1], and Jose Marengo[6]

[1]Jackson School of Geosciences, University of Texas at Austin, Austin, TX, USA, [2]Department of Atmospheric and Oceanic Sciences, University of California, Los Angeles, CA, USA, [3]Pacific Northwest National Laboratory, Richland, WA, USA, [4]Institute for Climate and Global Change Research and School of Atmospheric Sciences, Nanjing University, Nanjing, China, [5]Collaborative Innovation Center of Climate Change, Nanjing, China, [6]Centro Nacional de Monitoramento e Alertas aos Desastres Naturais, São Jose dos Campos, Brazil

Abstract We evaluate the Community Atmosphere Model Version 5 (CAM5) with a higher-order turbulence closure scheme, named Cloud Layers Unified By Binomials (CLUBB), and a Multiscale Modeling Framework, referred to as the "superparameterization" (SP) with two different microphysics configurations to investigate their influences on rainfall simulations over southern Amazonia. The two different microphysics configurations in SP are the one-moment cloud microphysics without aerosol treatment (SP1) and two-moment cloud microphysics coupled with aerosol treatment (SP2). Results show that both SP2 and CLUBB effectively reduce the low biases of rainfall, mainly during the wet season, and reduce low biases of humidity in the lower troposphere with further reduced shallow clouds and increased surface solar flux. These changes increase moist static energy in the lower atmosphere and contribute to stronger convection and more rainfall. SP2 appears to realistically capture the observed increase of relative humidity prior to deep convection, and it significantly increases rainfall in the afternoon; CLUBB significantly delays the afternoon peak rainfall and produces more precipitation in the early morning, due to more gradual transition between shallow and deep convection. In CAM5 and CAM5 with CLUBB, occurrence of more deep convection appears to be a result of stronger heating rather than higher relative humidity.

1. Introduction

The Amazonian rainforest, as a significant component of the global carbon cycle, accounts for approximately 15% of global terrestrial photosynthesis (Field et al., 1998). Changes of precipitation in this region in the 21st century would not only influence regional water and energy balance but also the global carbon-climate feedbacks and atmospheric CO_2 concentration (Cox et al., 2004). However, state-of-the-art climate models have been shown to have large biases in reproducing the rainfall climatology in the recent past and large intermodel spread in projecting future rainfall changes over Amazonia (Fu et al., 2013; Li et al., 2006; Vera et al., 2006; Yin et al., 2013). Such an inadequate representation of rainfall and its future changes in climate models has been a major source of uncertainty in projecting future atmospheric CO_2 concentration and resultant climate changes (Friedlingstein et al., 2006, 2014).

Significant low-precipitation biases were first found among nearly all climate models that participated in the Coupled Model Intercomparison Project (CMIP) phase 3 (CMIP3) of the World Climate Research Programme (WCRP), including the National Center for Atmospheric Research (NCAR) Community Atmosphere Model (CAM). Such a low-rainfall bias was at that time attributed to their underestimation of the surface latent flux (e.g., Li et al., 2006). However, despite improved surface latent flux in the CMIP Phase 5 (CMIP5), the low-rainfall biases still exist (e.g., Yin et al., 2013). In particular, in the Community Climate System Model version 4 (CCSM4) (Gent et al., 2011), a global climate model widely used by the research community in the United States, rainfall is underestimated over southern Amazonia despite its overestimation of the surface latent flux.

The low-rainfall biases over Amazonia in the global climate models can be a result of multiple factors. For example, Li et al. (2006) found that the simulated El Niño-like sea surface temperature (SST) pattern and warm bias in the northern tropical Atlantic appear to enhance atmospheric subsidence and consequently reduce

clouds and rainfall over the Amazon. Yin et al. (2013) speculated that the underestimation of cloudiness, which causes an overestimation of surface net radiative flux and resultant high biases of sensible flux and Bowen ratio, could contribute to the low-rainfall biases. Whether the underestimation of cloudiness is a result, rather than the cause, of the underestimation of rain bearing atmospheric convection remains unclear.

This study aims to test the response of rainfall over southern Amazonia, where the low-rainfall bias is centered, to several treatments of convective and cloud processes, and of the atmospheric boundary layer, in the Community Atmosphere Model version 5 (CAM5), a widely used global atmosphere model of the Community Earth System Model (CESM) developed at NCAR (Neale et al., 2010). CAM5 also shows low-rainfall biases similar to those of other CMIP3, CMIP5, and Atmospheric Model Intercomparison Project (AMIP) models, as will be shown in this paper.

Cumulus parameterizations in current global climate models do not represent deep convection and shallow-to-deep convection transition processes well enough and tend to underestimate rain rate with an early diurnal peak over land (e.g., Dai et al., 1999; Sato et al., 2009). These biases can be largely removed by resolving convective processes at a resolution finer than 5 km (e.g., Sato et al., 2009; Warner et al., 2003). However, it is computationally expensive and technically challenging to resolve convective processes, particularly in global models. As an intermediate step, Khairoutdinov and Randall (2001) and Grabowski (2001) developed a super-parameterization (SP) approach, which resolves convective process using a two-dimensional cloud-resolving model (CRM) embedded in each global climate model grid column, with a horizontal grid spacing of 1–4 km and about 24 vertical layers (Grabowski, 2001; Khairoutdinov & Randall, 2001).This approach has been shown to improve rainfall intensity on global scales (Kooperman et al., 2016), representation of the convective variability associated with the Madden-Julian Oscillation (Benedict & Randall, 2009), Asian and West African Monsoons (DeMott et al., 2011; McCrary et al., 2014), and organized convective systems over the Great Plains of the United States (Kooperman et al., 2013; Pritchard et al., 2011). Over South America, Krishnamurthy and Stan (2015) have shown that SP embedded in the Community Climate System Model Version 3 (CCSM3) can improve intraseasonal and interannual variabilities and their spatial pattern of rainfall associated with Pacific influences. To our knowledge, whether the SP approach can improve the diurnal cycle and reduce the low-rainfall bias over Amazonia has not been reported in past literature.

Both observations and numerical model experiments have suggested that aerosols could influence cloud microphysics and thus rainfall intensity over Amazonia (e.g., Andreae et al., 2004; Chakraborty et al., 2016; Koren et al., 2004, 2008; Lin et al., 2006; Martin et al., 2016; Wendisch et al., 2016). Song et al. (2012) and Lim et al. (2014) found some positive impacts of including microphysical processes in the Zhang and McFarlane convection scheme (Zhang & McFarlane, 1995) in simulating precipitation, cloud liquid water path, and surface radiative fluxes in global and regional models. In CAM5, aerosols only influence cloud microphysics in their large-scale stratiform clouds. In SP, the explicit-cloud parameterized-pollutant (ECPP) approach (Gustafson et al., 2008; Wang et al., 2011b) uses statistics of cloud distribution, vertical velocity, and cloud microphysical properties provided by the cloud-resolving model to drive aerosol and chemical processing in all cloud types. Establishing whether this physically more realistic approach that includes the aerosol influence on convective clouds would reduce the low-rainfall bias over the Amazon should shed light on how aerosols affect rainfall in the region.

Recent studies suggest that shallow convection affects the development of deep convection by its moistening and destabilizing of the lower troposphere (e.g., Derbyshire et al., 2004; Grabowski & Moncrieff, 2004; Holloway & Neelin, 2009; Waite & Khouider, 2010). Analyses of observations, including those from the recent GoAmazon field campaign, have shown that the development of shallow convection can influence the diurnal cycle and intensity of the deep convection over Amazonia (e.g., Zhuang et al., 2017). To improve the representation of the shallow convection and boundary layer clouds and thermodynamic processes, a third-order turbulence closure parameterization called Cloud Layers Unified by Binomials (CLUBB) (Golaz et al., 2002; Larson & Golaz, 2005) has been developed and implemented into CAM5 to provide a unified treatment of atmospheric boundary layer (ABL) processes, i.e., planetary boundary layer turbulence, shallow convection, and stratiform clouds (Bogenschutz et al., 2013). In a separate effort, CLUBB has also been implemented in the CRM component of SP to improve its turbulence and shallow convection treatment (Wang et al., 2015). Thus, we examine whether CLUBB can reduce the low-rainfall bias over Amazonia in both CAM5 and SP and, if so, through what process.

To isolate the influence of an improved representation of multiscale convective process, cloud microphysics, the ABL, shallow convective processes, and of aerosols, we will evaluate over southern Amazonia in section 3 six versions of CAM5, i.e., CAM5 (CM), CAM5 with CLUBB (CM_CL), SP with two-moment microphysics with aerosol treatment: SP2 and SP2 with CLUBB (SP2_CL), and SP with one-moment microphysics without aerosol treatment: SP1 and SP1 with CLUBB (SP1_CL). The influences of these processes on rainfall and bias in CAM5 and so potentially in CAM5-class global climate models will be discussed in section 4.

2. Models and Methodology

The CAM5.1 model and its SP version are used as bases in this study, with CLUBB implemented in both models. CAM5 was released in June 2010 as a component of the CESM developed at NCAR (Neale et al., 2010). Large-scale dynamics are treated using the Finite Volume dycore (Neale et al., 2010). CAM5 parameterizations include (i) the Zhang and McFarlane (1995) (ZM) scheme for deep convection with some further refinements documented in Neale et al. (2008), (ii) the Bretherton and Park (2009) shallow convection and moist turbulence schemes developed at the University of Washington (Park & Bretherton, 2009), (iii) a two-moment cloud microphysics scheme (Gettelman et al., 2008; Morrison & Gettelman, 2008) and a cloud macrophysics scheme (Park et al., 2014) for the parameterizations of clouds, and (iv) the open-source Rapid Radiative Transfer Model for General Circulation Models (GCMs) (RRTMG) package developed by Atmospheric and Environmental Research (Mlawer et al., 1997). Results from CM and CM_CL will be compared with results from the SP versions of CAM5.

CLUBB (Golaz et al., 2002; Larson & Golaz, 2005) has been developed and implemented into CAM5 to provide a unified treatment of boundary layer processes, i.e., planetary boundary layer turbulence, shallow convection, and stratiform clouds (Bogenschutz et al., 2013). This parameterization was developed assuming a joint probability density function (PDF) of vertical velocity, liquid water potential temperature, and total water mixing ratio at a particular location and time. Once the subgrid joint PDF is determined, the buoyancy terms, cloud fraction, cloud liquid water mixing ratio, and the unclosed moments can be diagnosed directly from it (Larson & Golaz, 2005). Although this PDF-based parameterization adds to the computational expense, it ensures consistency of cloud water content and cloud fraction and avoids artificial categorization of different cloud types (e.g., cumulus and stratocumulus) and physical processes (Larson et al., 2012).

The version of SP used in this study is documented in detail (Wang et al., 2015) (The source code of SPCAM used here can be found at https://svn-ccsm-models.cgd.ucar.edu/cam1/branches/spcam1_5_00_cam5_2_09_pnnl). Thus, we only briefly describe it here. The SP is an extension of the Colorado State University (CSU) Multiscale Modeling Framework model (Khairoutdinov et al., 2008, 2005; Li et al., 2009; Tao et al., 2009) that was first developed by Khairoutdinov and Randall (2001). The host GCM in SPCAM has been upgraded to the CAM5, and the resulting SP treats multiscale interactions of aerosols, clouds, and precipitation (Wang et al., 2011a, 2011b). The embedded CRM in each GCM grid column is a two-dimensional version of the System for Atmospheric Modeling (SAM) (Khairoutdinov & Randall, 2003). Convection is assumed to be resolved in the SP models; i.e., large-scale and convective rainfall are not generated by separate schemes but rather produced by the embedded CRMs. During each GCM time step (every 10 min), the CRM is forced by the large-scale temperature and moisture tendencies arising from GCM grid-scale dynamical processes and it feeds the cloud response back to the GCM grid scale as heating and moistening terms in the large-scale budget equations for heat and moisture. The CRM runs continuously using a 20 s time step with cyclical boundary conditions within each cell.

CLUBB has been further implemented into the CRM component of this version of SPCAM with its two different microphysical configurations (Wang et al., 2015), i.e., (a) the two-moment cloud microphysics scheme (Wang et al., 2015) ("SAM2MOM") that uses the Explicit Clouds Parameterized Pollutants representation of cloud effects on the aerosol (Wang et al., 2011b) and (b) the single-moment cloud microphysics scheme with no aerosol treatment. The CRM uses the radiation scheme used in CAM, Version 4 (Collins et al., 2004; Khairoutdinov & Randall, 2001; Khairoutdinov et al., 2005, 2008). There are some adjustments to both the single-moment (SAM1MOM) and two-moment (SAM2MOM) cloud microphysics schemes when they are coupled to CLUBB due to the fractional cloudiness that it diagnoses (Wang et al., 2015). To reduce computational expense, CLUBB is activated every third CRM time step; thus, the time step that CLUBB uses is 1 min.

Tendencies output from the CLUBB at each of its time steps are applied uniformly over all three CRM time steps (Larson et al., 2012). For other technical details, refer to Wang et al. (2015).

In this study, we perform six model experiments, i.e., CAM5 (CM), CAM5_CLUBB (CM_CL), MMF with two-moment microphysics (SPCAM_SAM2MOM (SP2) and SPCAM_SAM2MOM_CLUBB (SP2_CL)), and MMF without aerosol treatment (SPCAM_SAM1MOM (SP1) and SPCAM_SAM1MOM_CLUBB (SP1_CL)). The simulations are performed for 10 years with SST prescribed as climatology. The models are run at a horizontal resolution of 1.9° × 2.5° with 30 vertical levels. The embedded CRM includes 32 columns at 4 km horizontal grid spacing and 28 vertical layers coinciding with the lowest 28 CAM levels. The model aerosol treatment with a three-mode representation is chosen, as documented in Liu et al. (2012).

We use several observational data sets and reanalysis to compare with the results from the six models. The rainfall data sets are the monthly data from the Global Precipitation Climatology Project (GPCP) for the years of 1979–2014 (Adler et al., 2003; http://precip.gsfc.nasa.gov/) and 3-hourly data from Tropical Rainfall Measuring Mission (TRMM) for the years of 1998–2014 (Kummerow et al., 2000). The TRMM latent heating data used in this study is given by the TRMM 2H25 product for monthly profiles and 3G25 product for 3-hourly profiles, both of which provide 19 vertical levels of latent heating data derived using the Spectral Latent Heating algorithm (SLH) at each orbital grid point along the TRMM precipitation radar's swath. Radiative fluxes are from the Clouds and Earth's Radiant Energy System (CERES) Energy Balanced and Filled (EBAF) Edition 4.0 for the years of 2000–2014 (http://ceres.larc.nasa.gov). ERA-Interim is a reanalysis spanning from 1979 to present (Dee et al., 2011). The Modern-Era Retrospective Analysis for Research and Applications (MERRA) reanalysis has been produced by the Global Modeling and Assimilation Office of NASA, based on the Goddard Earth Observing System, version 5 (GEOS-5) (Rienecker et al., 2011), and covering the satellite era (1979 to present).

3. Results

3.1. Climatological Behavior

Figure 1 shows the climatological rainfall biases relative to GPCP rainfall data during October–March for the six different models (Table 1). In CM, large dry biases can be observed in the southern Amazonia region, while with CLUBB, these biases are significantly alleviated. With the superparameterization, the two-moment configuration SP2 decreases the dry biases but over the eastern tropical South America increases the wet biases. With the one-moment configuration, SP1 shows stronger dry biases than CM, but its dry bias is replaced by wet bias when it is coupled with CLUBB. Such a large swing between dry and wet biases shows a strong sensitivity of rainfall to the treatment of cloud microphysics and atmospheric boundary layer processes and shallow convection.

The root causes of the differences among the six versions of the CAM5 are their treatments of convective and cloud processes, the atmospheric boundary layer (ABL), shallow clouds, and the influence of aerosols on clouds. However, resultant changes of rainfall and clouds lead to changes of diabatic heating, which drive changes in the large-scale circulation and advection between different versions of CAM5 (Figure 1). The resultant moisture transport can provide feedback to rainfall differences; i.e., the initial rainfall and cloud changes among the six versions of CAM5 induced by different convective and cloud treatments can be further influenced by changes of the large-scale circulation. Thus, the changes of rainfall shown in Figure 1 are a combination of initial influences of the changes of convective and cloud processes and feedbacks between large-scale circulation and rainfall. In particular, the southeasterly wind biases and moisture divergence at 850 hPa within the southern Amazon domain in CM, CM_CL, SP1, and SP1_CL (Figures 1c–1h) are consistent with underestimate of rainfall over the southern Amazon and overestimate of rainfall in the Caribbean Sea or the equatorial Amazon (Wang & Fu, 2002). Likewise, the northwesterly wind biases in SP2 and SP2_CL (Figures 1e and 1f) are consistent with reduced low-rainfall biases in the southern Amazon domain and wet bias in the South American Convergent Zone over southeastern Brazil. While the reductions of the rainfall biases are robust and significant, we note that such changes among different CAM5 versions are partially influenced by the shifts of the bias to outside of our analysis domain (Figures 1e, 1g, and 1h). An increasing of domain size for analysis would likely reduce the rainfall differences among the different versions of CAM5, as implied by Figure 1, but it will also mix the regions with different rainfall seasonality.

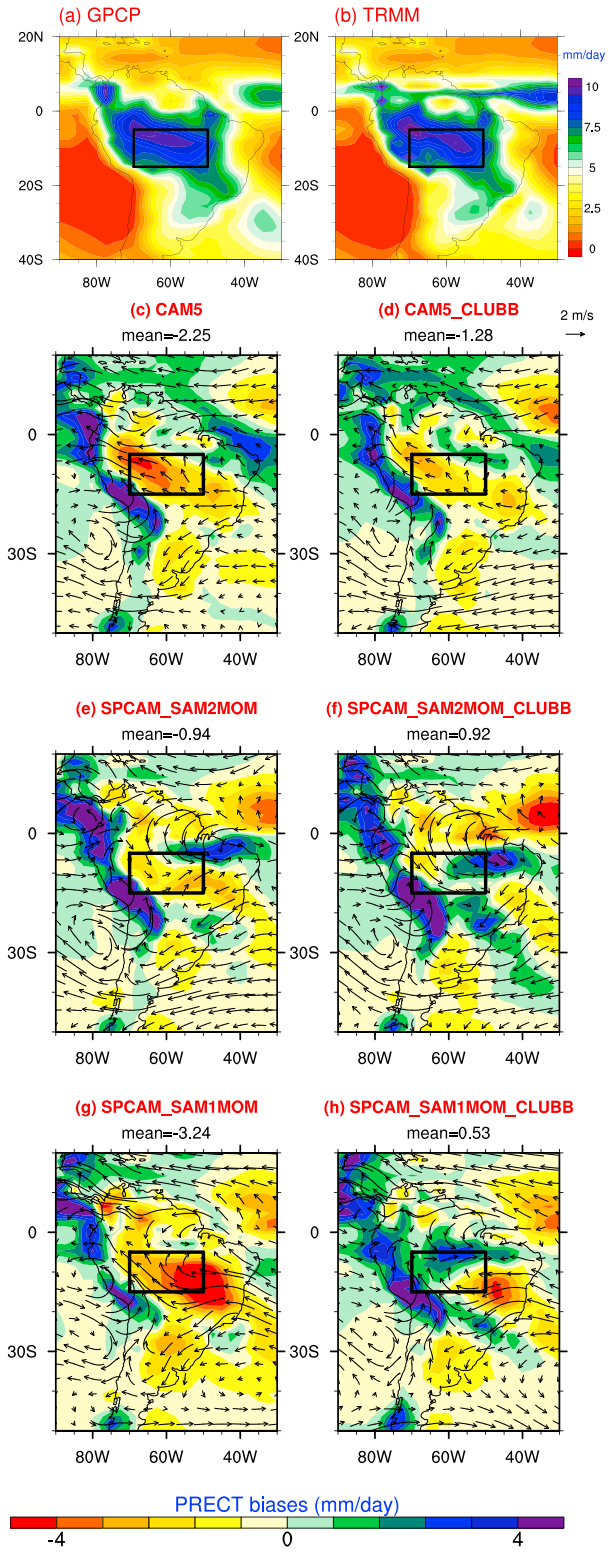

Figure 1. Climatological rainfall (mm/d) during the wet season (October–March) of (a) GPCP and (b) TRMM observations. Climatological precipitation biases (mm/d) during the wet season (October–March) of (c) CM, (d) CM_CL, (e) SP2, (f) SP2_CL, (g) SP1, and (h) SP1_CL compared with GPCP. Overlaid vectors are wind biases at 850 hPa compared with ERA-Interim reanalyses. The black box denotes the study region (5°–15°S, 50°–70°W).

Figure 2 shows the seasonal cycle of temperature, humidity, precipitation, clouds, radiative fluxes, and surface fluxes over the southern Amazon domain (5°S–15°S, 50°–70°W) in the six model configurations and observations. Figure 2a shows that CM has dry biases for precipitation simulations over the southern Amazon domain during both wet and dry seasons. CLUBB consistently reduces the dry bias in CM, SP2, and SP1 in the wet season (November–March). SP models show a strong sensitivity to cloud microphysics, i.e., only SP2 alleviates the dry biases of precipitation during the wet season. SP2_CL produces the most rainfall among the six models. SP1 worsens the dry bias compared to that of CM. Note that dry biases during the dry season (May–August) and the dry-to-wet transition season (September–October) remain. Such dry biases during the dry season occur in most of the CMIP5 models in both the southern and northern Amazon (Yin et al., 2013).

Because of the strong interdependence between precipitable water, clouds, rainfall, and land surface conditions, we evaluate how seasonal cycles of clouds and surface fluxes vary among the six models. We first evaluate whether their dry rainfall biases are due to lack of moisture in the atmosphere, as represented by precipitable water. Figure 2b shows that precipitable water is not underestimated in the wet season and that the models with the least dry rainfall bias, SP2_CL and SP1_CL, have the highest precipitable water. However, in the dry season, all the models have severely underestimated precipitable water. It does not vary with the different treatments of shallow and deep convection in the dry season. However, the models with the smallest dry bias in the wet season, i.e., SP2 and SP2_CL, also show a more rapid increase of precipitable water with the dry- to wet-season transition during September–October. Figure 2c shows that all six model configurations realistically represent the surface temperature during wet season (November–April) but overestimate its value during the late dry season and the dry to wet transition season (July–October). CM_CL reduces such warm surface temperature bias compared to CM. SPs, especially SP1, strongly exacerbate this warm bias in the surface temperature. CL has mixed effect in reducing this warm surface temperature bias in SP: it only reduces the warm bias in SP1.

Figures 2d and 2e show large spreads in surface sensible and latent heat fluxes, respectively, in both reanalyses and the six models, leading to large uncertainties in the assessment of the model behavior on surface fluxes. Most of those models fall within the range of different reanalyses, especially for the surface sensible flux (Figure 2d). Surface latent flux is underestimated during the dry season (June–August) beyond the range of observational uncertainty (Figure 2e). The models with least rainfall bias during the wet season, i.e., SP2_CL, SP2, and SP1_CL, produce largest surface latent heat flux at that time (November–May, Figure 2e). The variations of the sum of surface sensible and latent flux simulated by the six models are within the range of the observational uncertainty, except for CM, CM_CL, and SP1 during Septmeber–November, the dry to wet transition season (Figure 2f).

The surface solar flux (Figure 2g) is overestimated in all six versions during the dry and dry to wet transition seasons (May–October) compared to both CERES-EBAF observation and ERA-Interim. CM and CM_CL show the least overestimate of the surface solar flux, SP2 and SP2_CL increase its high bias, and SP1 and SP1_CL make it even worse. During the wet season (November–April), the modeled solar fluxes are within the range of the observational uncertainties as indicated by ERA-Interim and CERES-EBAF. The intermodel

Table 1
Cloud Treatments in Different Model Configurations, Revised From the Table 1 of Wang et al. (2015)

	Cloud treatment			Aerosol treatment	Radiation schemes
Case name	Deep convection	Shallow convection	Stratiform clouds and turbulence	Cloud processing of aerosols	
CAM5 (CM)	ZM[a]	UW[b]	UW with MG[c]	Parameterized clouds[d]	RRTMG in CAM5[e]
CAM5_CLUBB (CM_CL)	ZM[a]	CLUBB with MG[f]	CLUBB with MG[f]	Parameterized clouds[d]	RRTMG in CAM5[e]
SPCAM_SAM2MOM (SP2)	Explicitly simulated using SAM with the two-moment microphysics scheme; subgrid transport is treated using a simple Smagorinsky-type scheme; no subgrid cloud treatment			ECPP with no fractional cloudiness from SAM[g]	RRTMG in CAM5[e]
SPCAM_SAM2MOM_CLUBB (SP2_CL)	Same as SPCAM, but CLUBB is used to treat both subgrid transport and subgrid clouds			ECPP with fractional cloudiness from SAM[h]	RRTMG in CAM5[e]
SPCAM_SAM1MOM (SP1)	The same as SPCAM_SAM2MOM, but with the one-moment cloud microphysics scheme			ECPP with no fractional cloudiness from SAM[g]	CAM version 4[i]
SPCAM_SAM1MOM_CLUBB (SP1_CL)	The same as SPCAM_SAM2MOM_CLUBB, but with the one-moment cloud microphysics schemes			ECPP with fractional cloudiness from SAM[h]	CAM version 4[i]

[a]The deep convection scheme in both CM and CM_CL is based on Zhang and McFarlane (1995) (ZM) with some further refinements documented in Neale et al. (2008). [b]The shallow convection scheme in CM is from the University of Washington (UW) without detailed cloud microphysics (Park & Bretherton, 2009). [c]The treatments of stratiform clouds and turbulence in CM are from the University of Washington (Bretherton & Park, 2009; Park & Bretherton, 2009) coupled with the detailed Morrison and Gettelman (MG) cloud microphysics scheme (Morrison & Gettelman, 2008). [d]In CM and CM_CL, fields from conventional cloud parameterizations are used to treat cloud processing of aerosols (e.g., wet scavenging, aqueous chemistry, and convective transport) (Liu et al., 2012). [e]In CM, CM_CL, SP2, and SP2_CL, RRTMG in CAM5 is used for radiative transfer calculation. [f]In CAM5_CLUBB, CLUBB provides a unified treatment of shallow convection, stratiform clouds, and turbulence and is coupled with the MG microphysics scheme. [g]In SAM2MOM, cloud statistics from SAM is used to drive cloud processing of aerosols using the ECPP approach (Gustafson et al., 2008; *Wang et al.*, 2011a). No subgrid cloud treatment in SAM. [h]In SAM2MOM_CLUBB, the subgrid cloud treatment based on CLUBB in SAM is accounted for in ECPP. [i]The single-moment cloud microphysics scheme in the SAM CRM is coupled with the radiation scheme used in the CAM, version 4 (Khairoutdinov et al., 2005, 2008; Khairoutdinov & Randall, 2001).

variation of the surface solar radiation bias is in part consistent with that of the low cloud fraction (shown in Figures 2j and 4), i.e., CM and CM_CL overestimate high clouds and slightly underestimate low clouds compared to those of SP2, SP2_CL, SP1, and SP1_CL. This worsening of the high biases of surface solar radiation in SP1 and SP1_CL compared to SP2 and SP2_CL can be explained by their stronger reduction of high and middle level cloud fractions (cf. Figure 4). The surface net upward longwave flux is generally overestimated during both dry and wet seasons (Figure 2h). Such bias can be explained by the combined effects of warm biases at the surface and low biases of the precipitation, total column moisture, and cloudiness. The overestimate of surface solar is largely balanced by the overestimate of longwave fluxes during the dry season (Figure 2i), leading to relatively realistic net surface radiative flux (Figure 2i) and temperature (Figure 2c) during that season. However, during the dry to wet transition (September–November), overestimate of surface solar fluxes outweight that of longwave flux, leading to overestimate of surface net radiative flux (Figure 2i) that can explain the high bias of surface temperature during this period shown in Figure 2c.

How well do these models simulate clouds? Figure 2j shows that CLUBB can significantly decrease low clouds, consistent with Wang et al. (2015). This decrease leads to more shortwave fluxes to the surface, as shown in Figure 2g. Figure 2k shows that shortwave cloud forcing is not sufficiently negative during the wet season, compared with the CERES-EBAF observations. Generally, the models that strongly underestimate rainfall also underestimate cloud fraction (Figure 4) and underestimate shortwave cloud forcing in the wet season, i.e., CM and CM_CL. Underestimation of shortwave cloud forcing enhances net shortwave fluxes at the surface, leading to drier relative humidity and less precipitation. The longwave cloud forcing is underestimated during the dry and transition seasons, consistent with the underestimation of clouds implied by Figures 2g and 2k.

To give an overview of the biases of specific humidity, temperature, relative humidity, and vertical velocity, we show in Figure 3 the vertical profiles of these biases during the wet season in the six models compared with ERA-Interim reanalysis during the wet season. All the six models have dry biases in the lower troposphere and wet biases in the middle troposphere in terms of relative humidity (Figure 3c). Both CLUBB and SP2 reduce the dry biases in the lower troposphere (below ~750 hPa), while SP1 makes the lower troposphere even drier (Figure 3a). All the models have warm biases in the atmosphere, and this bias is strongest in SP2 and SP2_CL (Figure 3b). All the six models show strongly overestimated subsidence in the ABL (Figure 3d).

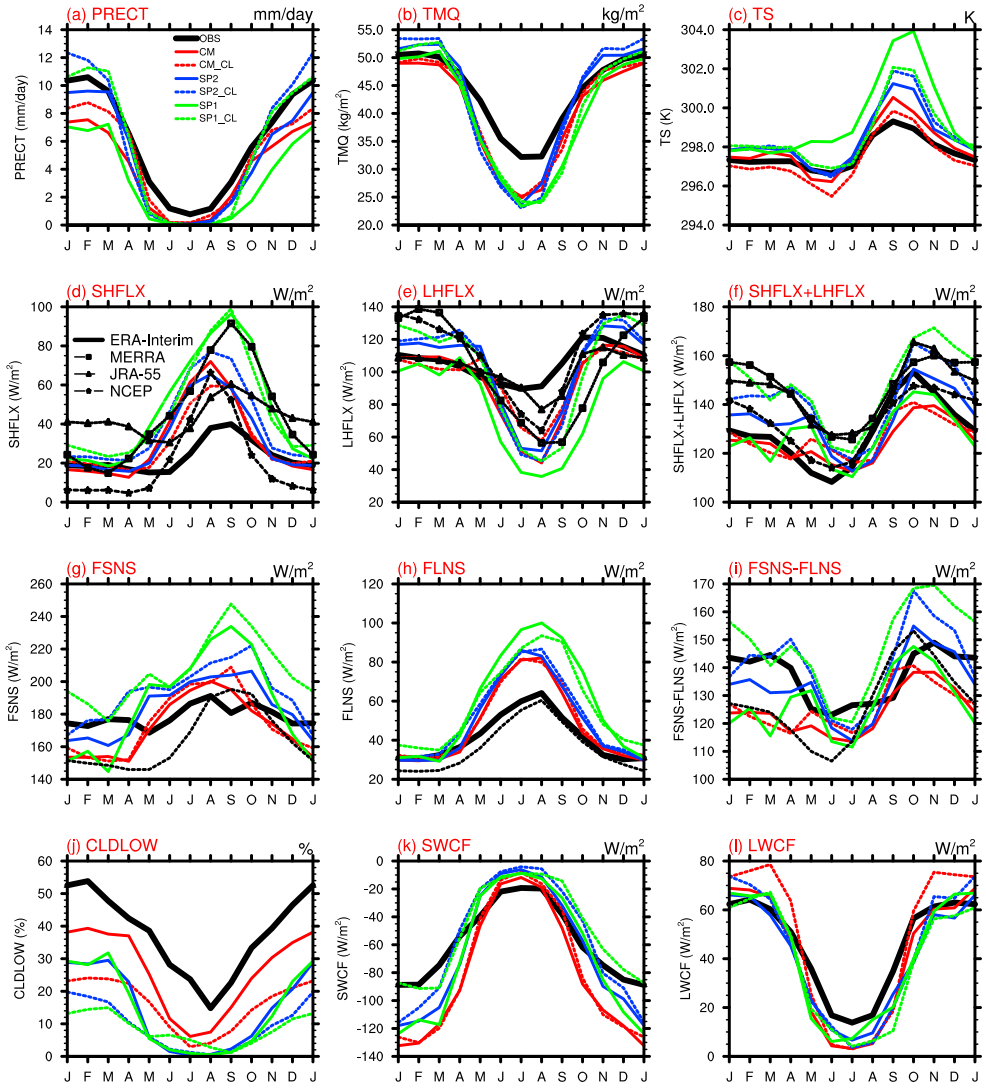

Figure 2. Seasonal cycle of (a) precipitation (PRECT, mm/d), (b) total precipitable water (TMQ, kg/m^2), (c) surface temperature (TS, K), (d) surface sensible heat flux (SHFLX, W/m^2), (e) surface latent heat flux (LHFLX, W/m^2), (f) sum of Figures 2d and 2e (SHFLX + LHFLX, W/m^2), (g) net solar flux at surface (FSNS, W/m^2), (h) net longwave flux at surface (FLNS, W/m^2), (i) difference of Figures 2g and 2h (FSNS − FLNS, W/m^2), (j) low cloud fraction (CLDLOW, %), (k) shortwave cloud forcing (SWCF, W/m^2), and (l) longwave cloud forcing (LWCF, W/m^2) over the southern Amazon domain from the observations and six models listed in Table 1. Observational data sets: precipitation is from GPCP; low cloud fraction is from Cloudsat; total precipitable water, surface sensible heat flux, and latent heat flux are from ERA-Interim; shortwave cloud forcing, net solar flux, and longwave flux at surface and longwave cloud forcing are from CERES-EBAF (dashed lines in Figures 2c and 2d are from ERA-Interim for comparison); and MERRA, JRA-55, and NCEP reanalyses are shown as black dashed lines in Figures 2d–2f.

SP1 and SP2 also overestimate the subsidence at the top of convection, which is consistent with the dry advection (Figure 3e) and underestimate of cloud fraction in the upper to middle troposphere (as will be shown in Figure 4). Both CLUBB and SP2 increase convection above the ABL (Figure 3d), which takes more moisture upward (Figure 3f). Almost all the models overestimate the moisture divergence above 850 hPa (Figure 3e), especially SP. However, the vertical components of moisture tendency in SP2 and SP2_CL overweigh the advective components, leading to more humidity in both models.

The effect of SP and CLUBB in CAM5 on cloud cover is investigated in Figure 4. Figure 4a shows that in the wet season CLUBB in CAM5 increases it in the middle and upper troposphere by as much as 20% and reduces it in the lower troposphere by as much as 10%, consistent with Figure 2j. However, CLUBB does not change cloud fraction during the dry season. CLUBB in SP2 increases cloud fraction in the upper troposphere by about 10%

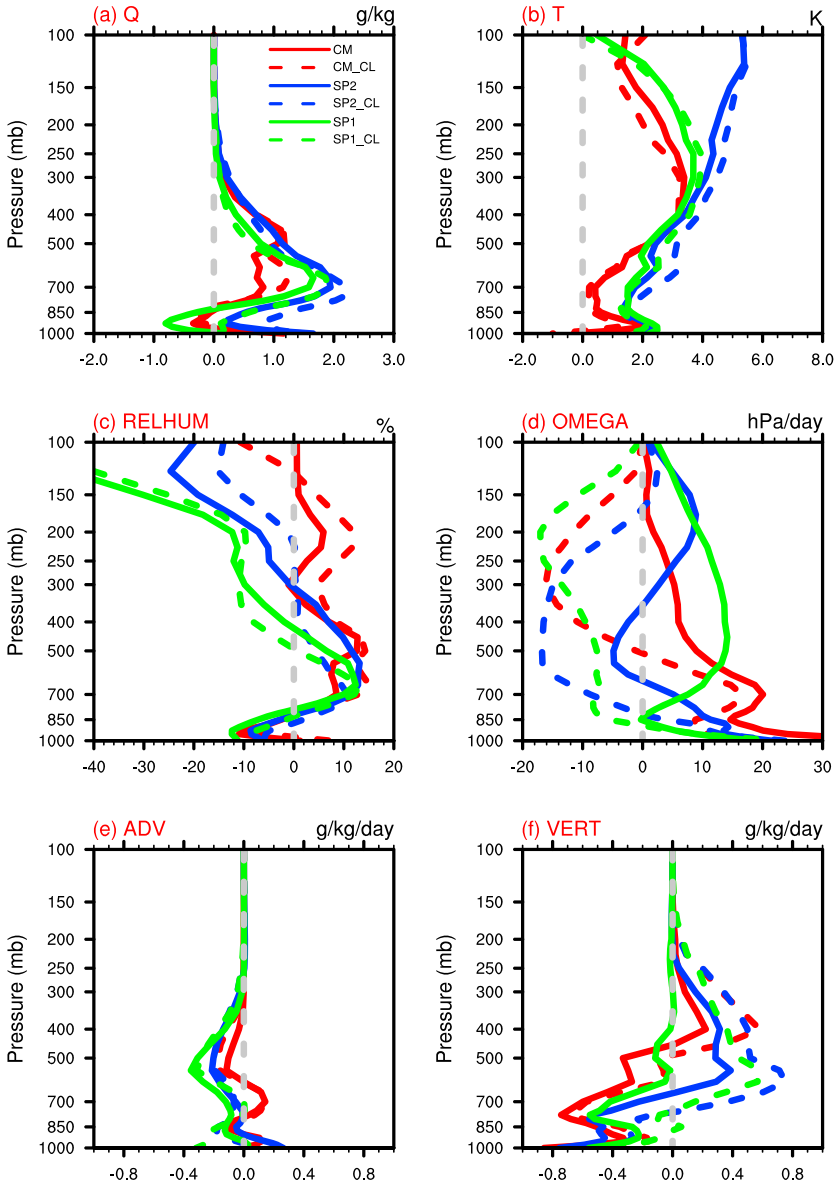

Figure 3. Vertical profiles of biases of (a) specific humidity (*Q*, g/kg), (b) temperature (*T*, K), (c) relative humidity (RELHUM, %), (d) vertical velocity (OMEGA, mbar/d), (e) advective moisture tendency term (ADV, g/kg/d), and (f) vertical moisture tendency term during the wet season (October–March) over the southern Amazon domain in the six models compared to those derived from with ERA-Interim.

relative to SP2 during the wet season (Figure 4b). CLUBB in SP1 appears to have the least impact on cloud fraction in the late wet season (December–April, Figure 4c), only increasing it by 5% in the upper troposphere. SP by itself leads to decreases of cloud fraction by as much as 20% above the lower troposphere during the wet season (Figures 4d and 4f), more for SP1. CL decreases cloud fraction during the wet season, most in SP2_CL, but also more in SP1_CL than in CM_CL (Figures 4e and 4g).

Figure 5 shows the latent heating profiles of the six models compared with TRMM observations and ERA-Interim and MERRA reanalyses. First, there are considerable uncertainties among the observation and reanalysis products. The TRMM observations show latent heating from 850 hPa to 200 hPa with maximum heating at 400 hPa during wet and dry to wet transition seasons (September–April) and 700 hPa during dry season. ERA-Interim does not have latent heating archived, so we use for it the total diabatic heating minus the radiative heating (Zhang et al., 2016). ERA-Interim shows latent heating from surface to higher than 150 hPa,

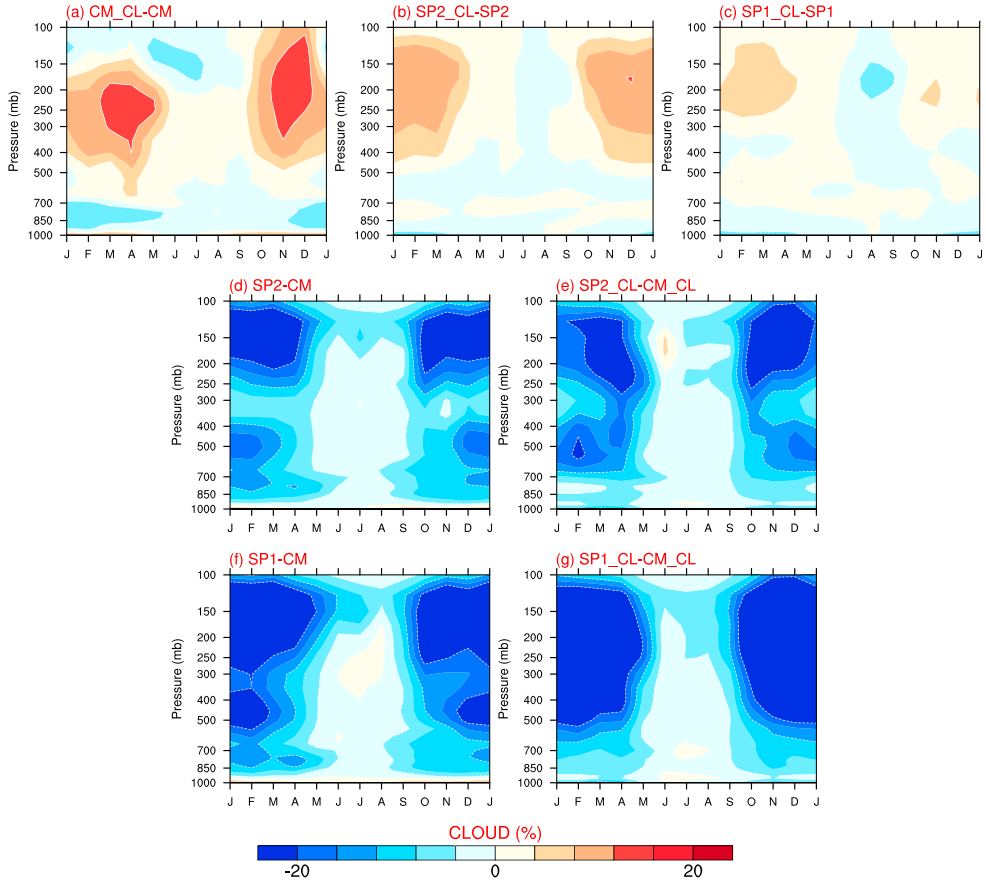

Figure 4. Seasonal cycle of cloud fraction differences over the southern Amazon domain between the six models. (a–c) The difference due to CLUBB; (d, e) the influence of SP2; and (f, g) the influence of SP1.

peaking around 500 hPa, during the wet season, slightly lower than that of TRMM (Figure 5b). Latent heating is much weaker and shallower, but still positive, during the dry season. Latent heating in MERRA (Figure 5c) is positive from the surface to 200 hPa, similar to that of the TRMM. However, its magnitude is weaker and peak is lower (700 hPa to 500 hPa) than that of TRMM. Based on Ling and Zhang (2013), both reanalyses show a shallower peak of atmospheric diabatic heating over the South American sector than that derived from atmospheric soundings. Although differences exist between TRMM observations and the two reanalyses, they have a common feature of gradual transitions during the wet-to-dry and dry-to-wet transition seasons.

In contrast, latent heating drops sharply to nearly 0 above 700 hPa in all six models, even weakly negative in SP2 and SP1 during the dry season (Figures 5d–5i). Below 700 hPa, CM shows nearly zero latent heating, whereas SP and CLUBB (CM_CL, SP2, SP2_CL, SP1, and SP_CL) lead to strong latent heating. During the dry- to wet-season transition (September–November), the CLUBB (CM_CL, SP2_CL, and SP1_CL) appears to improve the shallow-to-deep convection transition (Figures 5e, 5g, and 5i) but overestimates latent heating between 700 hPa and 300 hPa (Figures 5e, 5g, and 5i). During wet season, CM (Figure 5d) shows a relatively more realistic magnitude of the latent heating profiles than those of the four SP versions (Figures 5f–5i) and CM_CL (Figure 5e), although it overestimates the height of the latent heating compared to TRMM. The SP models produce much shallower latent heating than CM and CM_CL and some spurious latent cooling during the dry season (Figures 5f–5i). SP2 increases latent heating in the middle troposphere but decreases it in the upper troposphere (Figures 5f and 5g).

Figure 6 shows the observed and modeled probability density distribution of rainfall. Among the six models, CM shows the greatest overestimation of the light to medium rain rates and underestimation of heavy and extreme rain rate, whereas SP2_CL best captures the observed probability distribution of the rain rates, although it generates more extreme precipitation events compared with observations (Figure 6a). It does

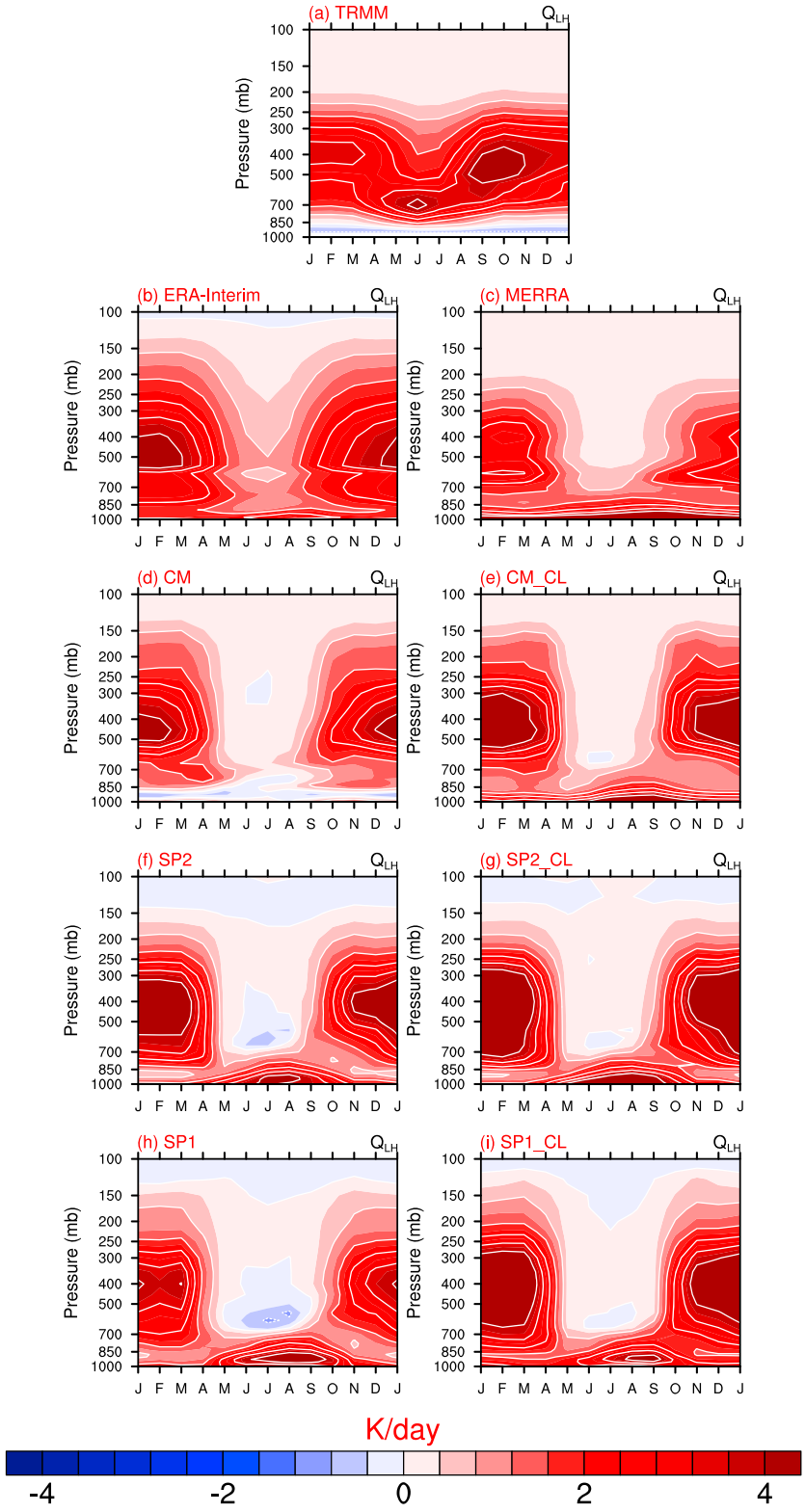

Figure 5. Seasonal cycle of latent heating over the southern Amazon domain in (d–i) the six models compared with (a) TRMM observations, (b) ERA-Interim, and (c) MERRA reanalyses.

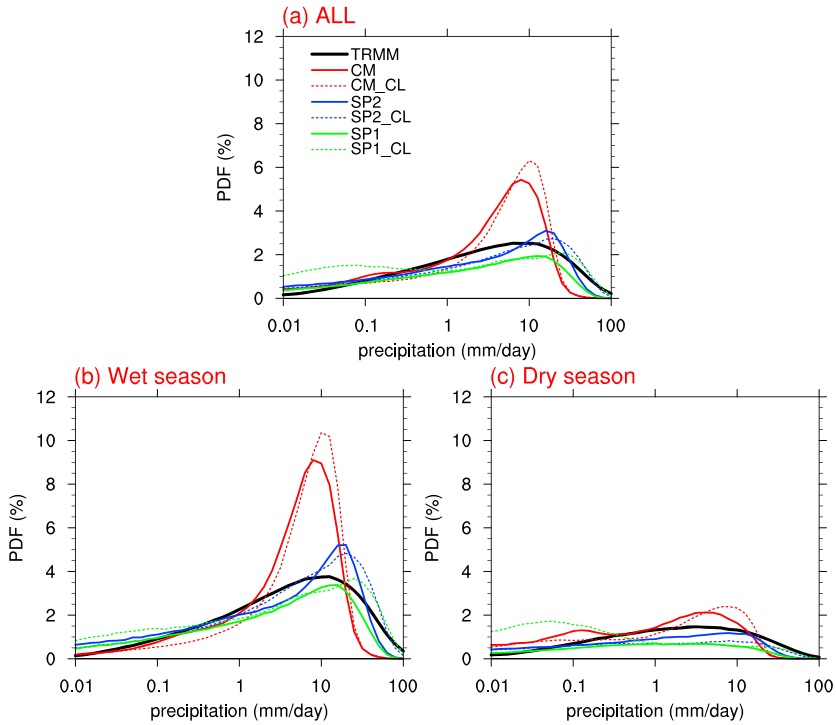

Figure 6. Probability density function of precipitation over the southern Amazon domain using 3-hourly data sets in the six models and observations during (a) all the year round; (b) the wet season; and (c) the dry season. Very light, light, medium, and heavy rain discussed in the text refer to the rain rate ranging between 0.01 and 0.1 mm/d, between 0.1 and 2.5 mm/d, between 2.5 and 10 mm/d, and >10 mm/d, respectively.

so because SP2 substantially reduces the overestimation of light and medium rain rate, and CLUBB further increases the frequency of heavy rain rates in the wet season (Figure 6b). In contrast, SP1 substantially overestimates the frequency of light rain and underestimates the frequency of rain rates at all other intensities in the wet season (October–March, Figure 6b). CLUBB in SPs further exacerbates the overestimation of light rain but increases the frequency of heavy to extreme rain rates in the wet season (Figure 6b). These changes of wet-season rain rates are the main contributors to the changes of the annual rain rate probability distribution among the six models (Figure 6a). During the dry season (April–September), SP improves the shape of the rain rate probability distribution curves but underestimates rain rates frequency at moderate intensities and overestimates the frequency of light rain (Figure 6c). CLUBB in SP1 further exacerbates the overestimation of light rain. It also reduces the low bias of the peak rain rates in the wet season.

In summary, the results in Figures 1–5 suggest that SP and CLUBB in CAM5 can significantly improve rainfall and precipitable water by altering surface radiative fluxes, cloud forcing, and the latent heating profiles and weak convection above the ABL in the wet season relative to the original CAM5. In fact, SP can increase the surface solar flux, temperature, and latent heating in these seasons. For the wet season, both versions of SP appear to be most effective in improving the probability distribution of rain rates, and the rainfall amount, by reducing the frequency of light rain rates and increasing the frequency of medium to extreme rain rates. These improvements are rather sensitive to the microphysical treatment in SP. For example, while SP2 provides a more realistic rain rate and stronger latent heating, SP1 best captures the shape of the rain rate distribution curve. However, the SP models produce too shallow latent heating (below 250 hPa) during the wet season and too strong latent cooling during the dry season. CLUBB also moderately improves the rain rate probability distribution by increasing the frequency of heavy rain rates and vertical velocity in the tropospheric column.

3.2. Diurnal Cycle

Convection in climate models that have parameterized convection, including CAM5, tends to develop faster and die faster than observed, leading to an earlier and shorter duration bias of the diurnal peak rainfall. To

evaluate whether representation of the subgrid convective dynamics, as implemented by the SP models, and a unified treatment of planetary boundary layer turbulence, shallow convection, and stratiform clouds, as represented by CLUBB, could reduce such a bias, we evaluate against TRMM in Figure 7 the diurnal cycle of precipitation throughout the year over the south Amazon region in the six simulations. Here we use UTC time, which is 3 h later than the local time at Sao Paulo, Brazil (~ 46°W), and 4 h later than the local time at Manaus (~ 60°W). TRMM rain rate data shows that during the wet season, the most intense rainfall occurs in the late afternoon (~ 21 UTC time) and then decays gradually until the early morning (8–10 UTC) of the following day (Figure 7a). During the dry season, rainfall occurs infrequently and only in late afternoon. As shown in Figure 7b, CAM5 shows a daily maximum precipitation near noon (i.e., at ~16 UTC) during a day and a substantial underestimate of rain rate during the wet season. Rainfall decays in the late afternoon, rather than as observed at late night. The early morning rainfall during the wet season is thus also underestimated. During the dry season, virtually no rainfall is simulated, so its late afternoon peak is missing. CLUBB is able to improve the rainfall diurnal cycle by delaying the afternoon rainfall to ~18 UTC (i.e., by ~2 h) and producing more rainfall in early morning (Figure 7c), presumably due to its ability to better simulate the relation between the ABL and shallow clouds and thus moisture transport from the ABL to free troposphere. However, its rain rate is still substantially weaker than that observed. SP2 strongly increases the rain rate in the late afternoon and also produces morning rainfall during 6–10 UTC (Figure 7d). The intensity of afternoon rainfall in SP2 is close to that observed. However, the afternoon peak rainfall is still too early (~ 16–20 UTC) and somewhat stronger than observed. Also, the nocturnal rainfall seen in TRMM is largely missing. When combining SP2 with CLUBB (SP2_CL), the model produces the most realistic afternoon peak and more early morning rainfall, although it generates a spurious late morning rainfall (~12–16 UTC). The diurnal cycle of rainfall in SP1 and SP1_CL is similar to that in SP2 and SP2_CL but with much weaker rain rate for its afternoon peak. This result is consistent with its underestimation of medium to extreme rain rate distribution in the one-moment cloud microphysics without treatment of aerosols that is shown in Figure 6.

Latent heating profiles contribute to the influence of deep convection on the large-scale circulation. Thus, in Figure 8 we evaluate the diurnal altitude patterns of latent heating from the six models against TRMM observations and ERA-Interim and MERRA reanalyses during the late transition to wet season (October–March). TRMM shows a peak of latent heating at around 18 UTC hour, with 4–6 K/d between 700 and 350 hPa (Figure 8a). ERA-Interim shows a strong diurnal peak of deep latent heating in the troposphere in late afternoon, with 6–8 K/d between 700 and 350 hPa and 2–3 K/d between 300 and 200 hPa (Figure 8b), which is stronger than that of TRMM. From early morning to noon, there is also about 1–2 K/d latent heating centered between 600 and 300 hPa, which is weaker than seen in TRMM. In MERRA, the latent heating is shallower and weaker and peaks earlier than that in TRMM and ERA-Interim in the afternoon but deeper and stronger in the morning. The latent heating peaks near 500 hPa in both TRMM and ERA-I, where the freezing level is generally located. In MERRA, latent heating peaks somewhat below 500 hPa. In CM, the overall pattern is similar to that in TRMM, but the latent heating peaks in early afternoon with a rate smaller than that in TRMM and in the two reanalyses both between 600 and 300 hPa and at 200 hPa (Figure 8d). Such a weaker and lower diurnal peak of latent heating can result in a weaker response of the large-scale circulation to deep convection. CLUBB embedded in CM enhances the latent heating to 50% or more of that in the reanalysis and also reduces the latent cooling bias in the ABL (Figure 8e). SP2 increases the peak latent heating rate in early afternoon to values higher that of TRMM (Figure 8f). However, the time period of such peak latent heating is earlier than that of the TRMM and ERA-Interim. SP2 also produces spurious latent cooling below 850 hPa before and after the afternoon peak of latent heating. When CLUBB is added (SP2_CL, Figure 8g), the diurnal peak of latent heating is delayed. It also reduces the overestimate of diurnal peak heating rate by about 1.5 K/d. The spurious latent cooling below 850 hPa still exists. Finally, in SP1 (Figure 8h), the latent heating rate is reduced by ~40–50% relative to SP2, i.e., it is more comparable to the TRMM observations (Figures 8f and 8a). The spurious cooling below 850 hPa still exists. The impact of the cloud microphysical treatment appears to be less when CLUBB is included in SP1 (Figure 8i compared to Figure 8h) than in SP2 (Figure 8g compared to Figure 8f). SP1_CL retains a similar pattern of the diurnal cycle of the latent heating (Figure 8i) as that of SP2_CL (Figure 8g), although it reduces the magnitude of the peak latent heating rate by ~25% in late afternoon. The CM and CM_CL have their peak of latent heating at the freezing level (near 500 hPa, Figures 8d and 8e), whereas the four SP model versions do not (Figures 8h and 8i). Figure 8 suggests mixed effects of the SP and CL on improving the diurnal cycle of the latent heating profiles. While both SP1 and SP2 sharpen

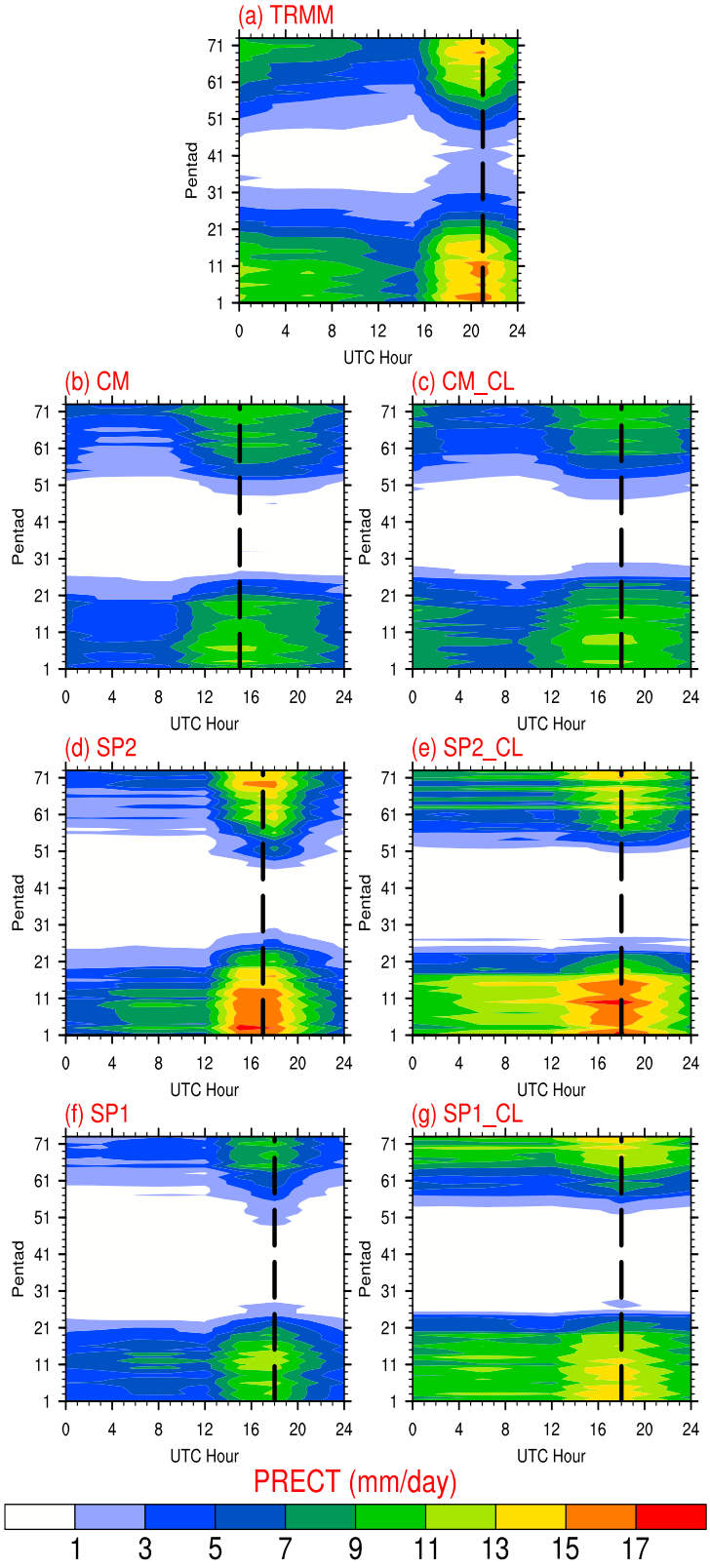

Figure 7. Diurnal cycle of precipitation (mm/d, horizontal axis) and its seasonal variation (vertical axis) over the southern Amazon domain from (b–g) the six models and (a) TRMM. The *x* axis is the Universal Time (UTC), and *y* axis is the date. The dashed black lines denote the hours when the peak precipitation occurs during each pentad. At 12 UTC is 8 A.M. local time at 60°W, the longitudinal center of the southern Amazon domain.

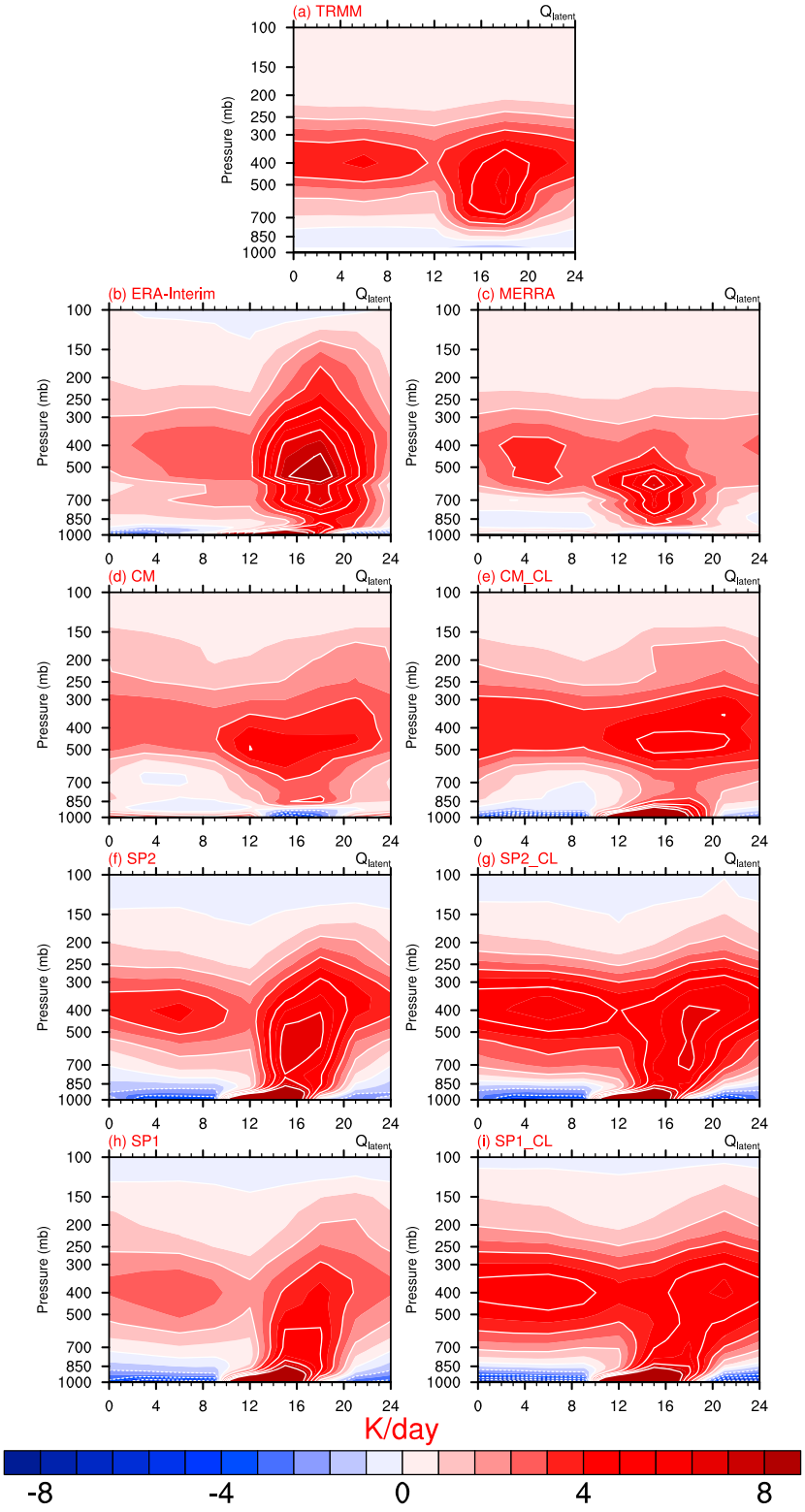

Figure 8. Diurnal cycle of latent heating during the wet season (October–March) in (a) TRMM, (b) ERA-Interim, (c) MERRA, and (d–i) the six models.

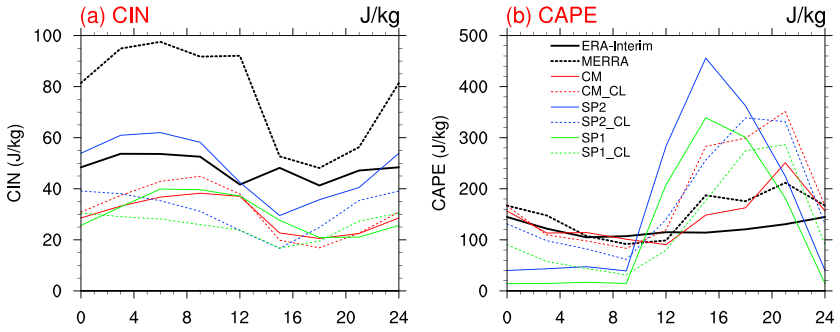

Figure 9. Diurnal cycle of (a) CIN and (b) CAPE in ERA-Interim, MERRA, and the six models during the wet season (October–March).

the afternoon peak of the latent heating profiles, they tend to overestimate the latent heating rate, create spurious latent cooling in the lower and upper troposphere in morning and evening, and remove the latent heating center near the freezing level. CL delays the afternoon peak of the latent heating and reduces the high bias of the latent heating rate induced by SP1 and SP2.

Figure 9 shows the diurnal cycle of CIN and CAPE in the six models, and for reference also that calculated from the two reanalyses, ERA-Interim and MERRA in the same way are also shown. CLUBB in CM decreases CIN and increases CAPE in the afternoon. In the SPs, CLUBB delays the peak of CAPE. SP2 increases both CIN and CAPE, especially in the afternoon, which promote quick development of deep convection; it decreases CAPE in the morning, which is consistent with the latent heating patterns shown in Figure 8f.

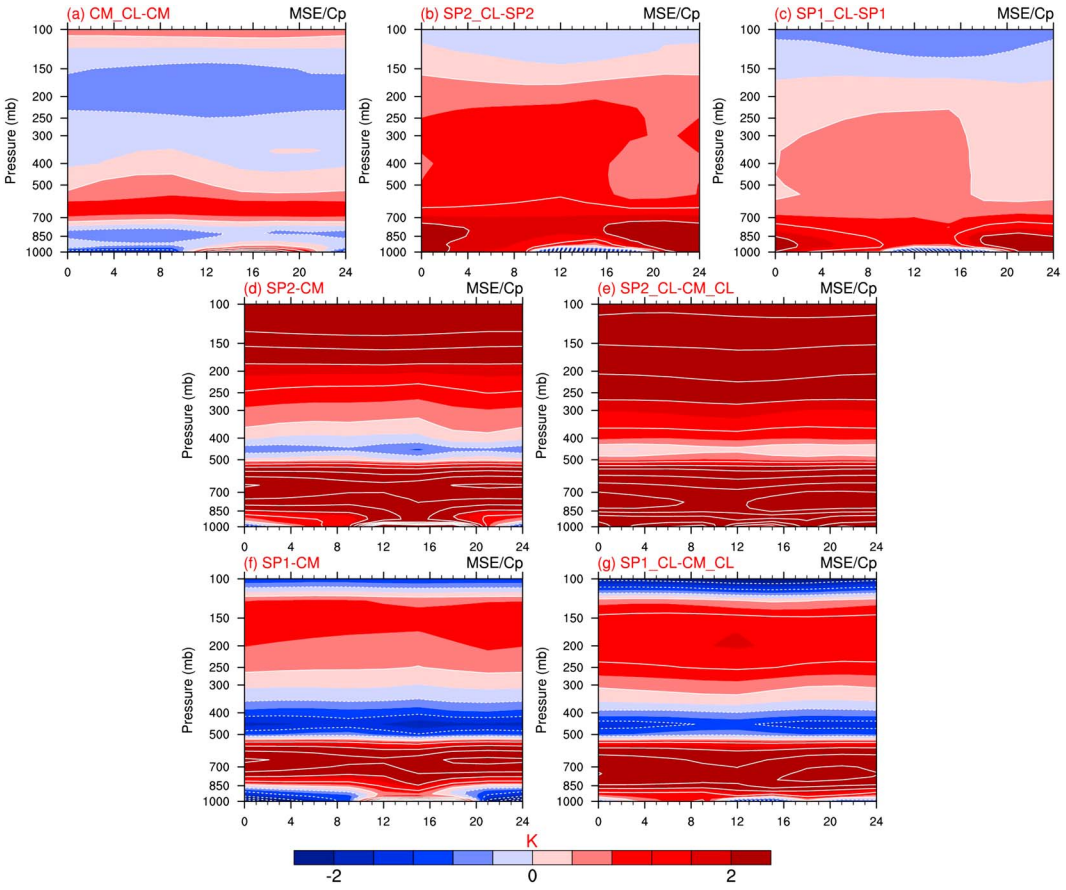

Figure 10. Changes of the diurnal pattern of MSE in CAM5 during the wet season (October–March) over the southern Amazon (a–c) due to CLUBB, (d, e) due to SP2, and (f, g) due to SP1.

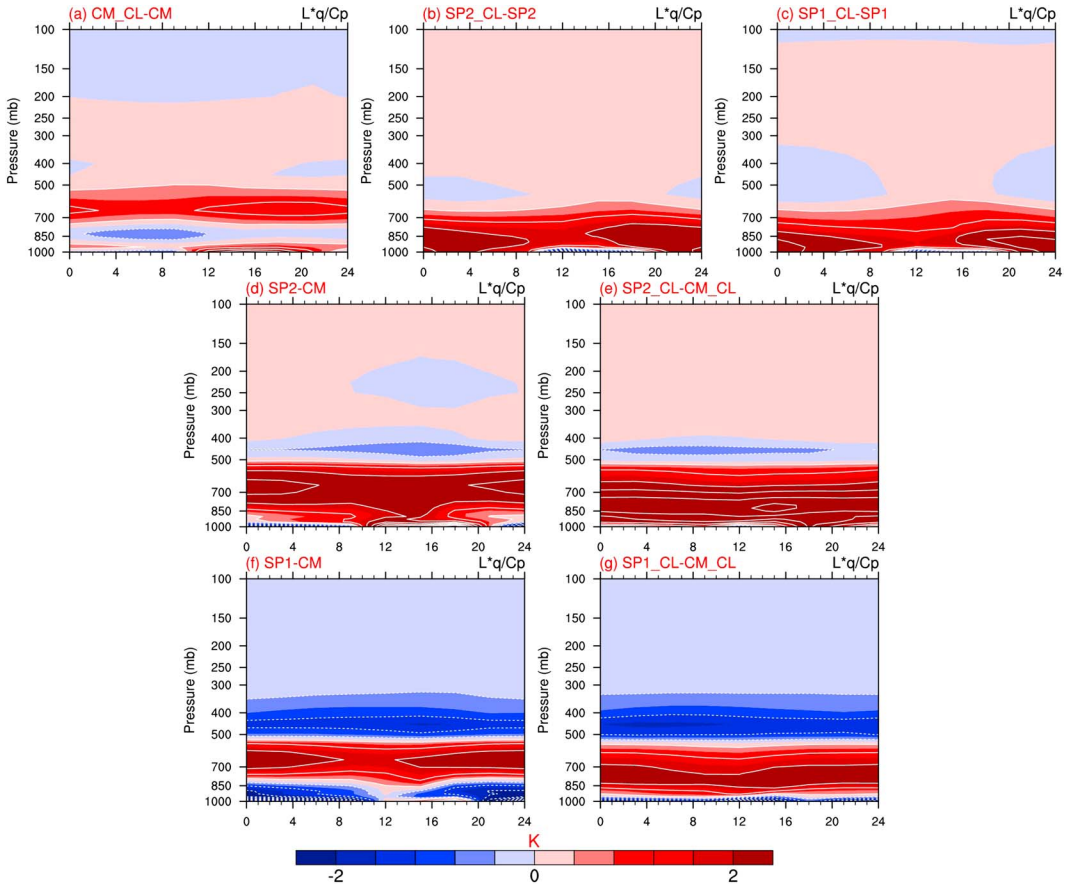

Figure 11. Same as Figure 10 but for moisture differences.

To understand whether the large-scale thermodynamic instability might cause the changes of rainfall behavior between the different treatments of convection in CAM5, we use moist static energy (MSE) to check the stability of the atmosphere in these models. The MSE is defined as MSE = $C_pT + L_vq + gz$, where C_p is specific humidity of dry air at constant pressure, T is temperature, g is gravity, z is geopotential height, L_v is latent heating of vaporization, and q is specific humidity. The MSE profiles indicate the stability of atmospheric columns based on the vertical distributions of temperature and moisture. A positive difference of MSE suggests that the atmosphere is more saturated, warmer, and less stable (more CAPE) and can generate more precipitation.

Figure 10 shows the difference of the diurnal cycle of MSE between pairs of models: CLUBB in CM decreases MSE in the lower atmosphere during the morning and increases MSE during the afternoon (Figure 10a); these differences are primarily due to the changes of moisture (Figure 11a). In the SP models, CLUBB acts to increase MSE during early morning and late evening (Figures 10b and 10c), when shallow convection dominates. This increase is primarily due to moisture increase (Figures 11b and 11c). Such higher MSE can contribute to the increase of rainfall during this period. With SP2, lower atmospheric MSE increases significantly throughout the day (Figures 10d and 10e), due to both higher humidity (Figures 11d and 11e) and temperatures (Figures 12d and 12e), but humidity dominates this increase in the ABL. This increase of MSE increases CAPE in the afternoon (Figure 9b). The instability of the atmosphere in SP2 and SP2_CL is the highest among all the models, leading to their higher rainfall in the afternoon (Figures 7d and 7e).

In terms of diurnal cycle of rainfall, SP significantly increases deep convection and precipitation in the afternoon, but it does not reduce the early bias of the diurnal peak of the rainfall as much as does CLUBB; CLUBB, on the other hand, improves the diurnal cycle of rainfall by delaying the afternoon peak time and producing precipitation in the early morning, due to a more gradual transition between shallow and deep convection.

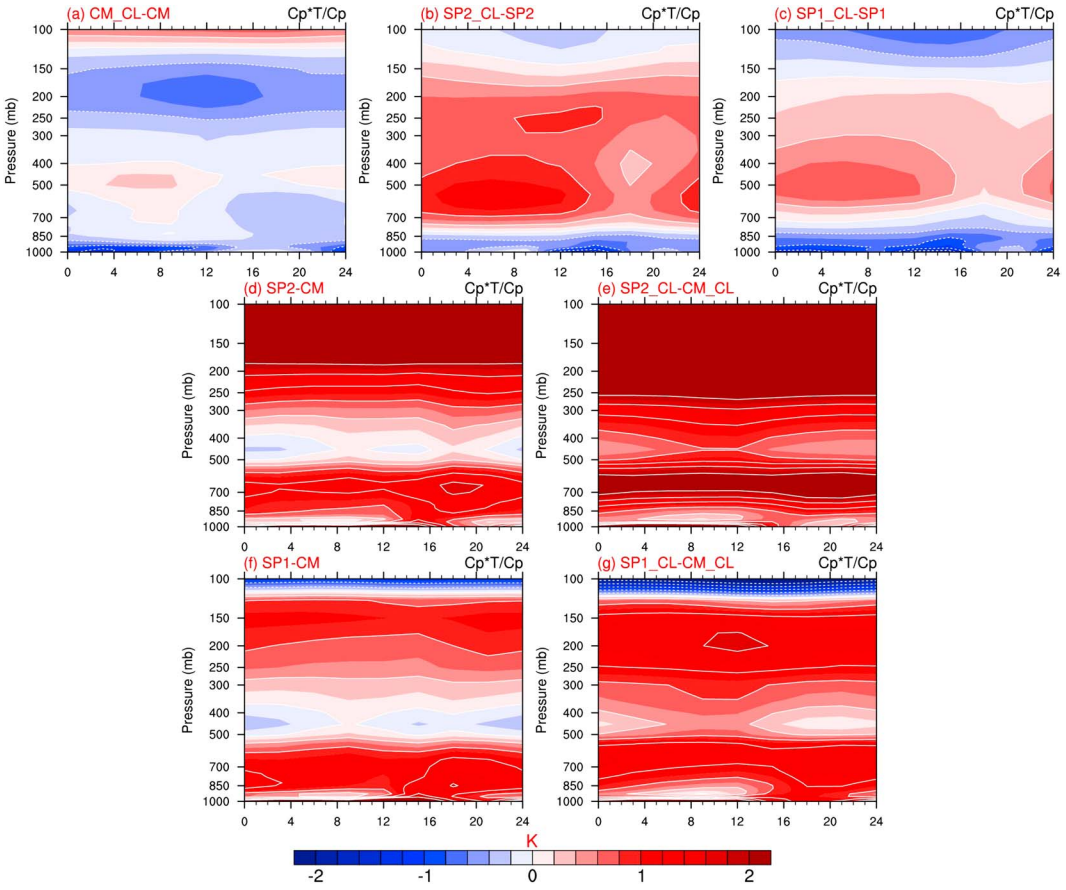

Figure 12. Same as Figure 11 but for temperature differences.

The SPs, especially SP2, can increase or even overestimate precipitation in the afternoon, but do not delay the timing of the precipitation peak as much as CLUBB.

3.3. Interaction Between Rainfall and Environmental Conditions

Convection represents a key adjustment process for large-scale atmospheric circulation. Thus, the realism of the interaction between convection and ambient large-scale atmospheric thermodynamic conditions represents the most important goal of the convective parameterization. Errors in representing such interactions can lead to rapid growth of the errors in both rainfall and large-scale circulation. To evaluate how well this interaction is represented in the models, we compare the composited atmospheric conditions before and after high- and low-precipitation events in Figures 13–15. Here high-rainfall occurrences are defined as the days with daily precipitation anomalies exceeding the one standard deviation thresholds. Only results of high-rainfall composites are shown here as low-rainfall composites are similar but of opposite signs. In observations, precipitation over the southern Amazon region follows anomalous high relative humidity in the entire tropospheric column that peaks in the middle troposphere, starting as much as 90 h before high-precipitation events (Figure 13a). The gradual deepening and strengthening of high relative humidity prior to the deep convection suggests a possible moistening effect of convective congestus and transition to deep convection. The moistening by strong rainfall also peaks in the middle troposphere during the 90 h after the peak rainfall events. In CM (Figure 13b), the anomalous increase of relative humidity prior to high-rainfall events is much weaker and confined to below 500 hPa. The sudden deepening of the high relative humidity (RH) layer suggests a lack of realistic transition from congestus to deep convection. The moistening by deep convection is also much stronger and deeper than that of the reanalysis. CLUBB reduces the low relative humidity bias prior to high-rainfall events (Figure 13c), but still produces a pattern of shallow moist layer similar to that of CM (Figure 13b). CLUBB further strengthens the overestimation of moistening of the deep tropospheric column after high-rainfall events in CM_CL (Figure 13d) and SP2_CL (Figure 13f),

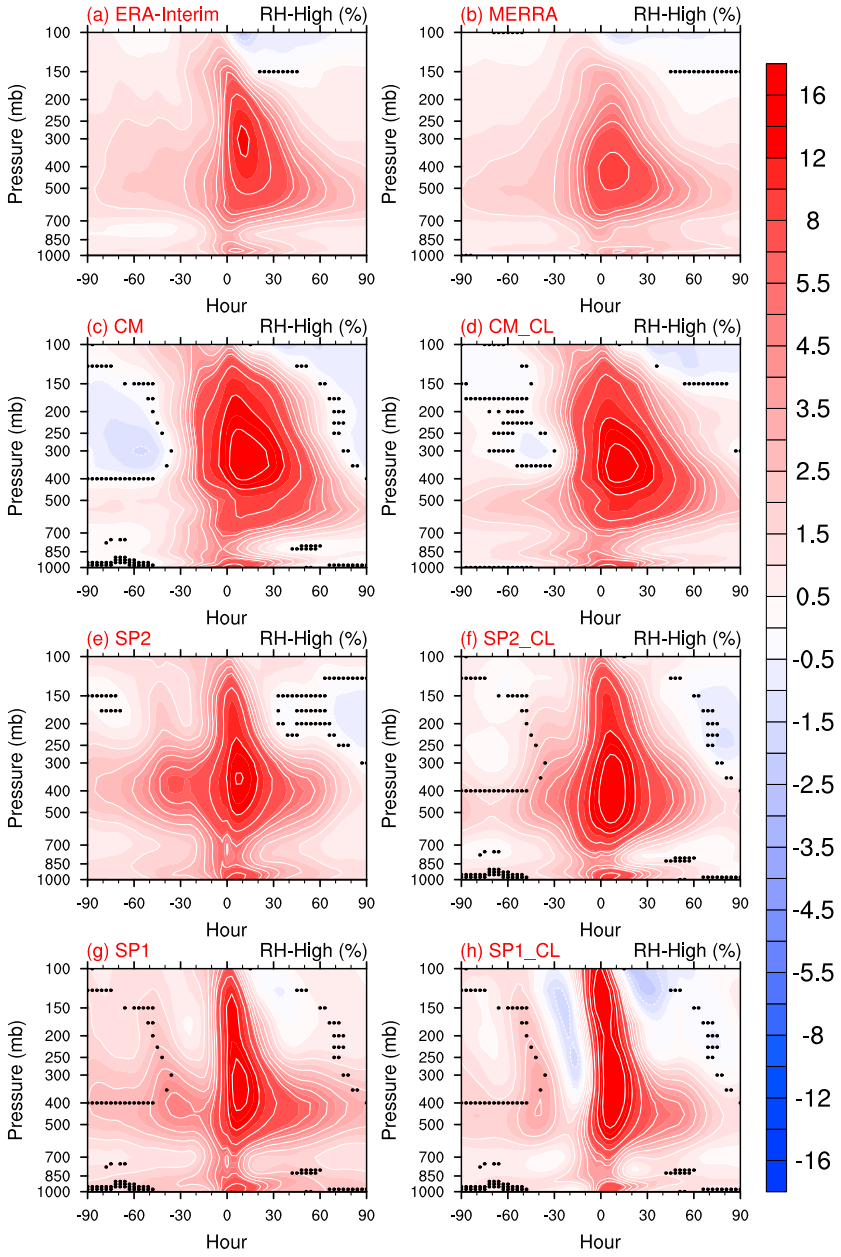

Figure 13. Time-vertical evolution of relative humidity anomalies (%) composited for high-precipitation events over the southern Amazon, derived from (a) ERA-Interim, (b) MERRA, and (c–h) six models. Precipitation data used for Figures 13a and 13b are from TRMM. The dots represent grids that are not significant at 95% level. The significance test is based on a bootstrapping method by permuting the original time series for 10,000 times.

compared to that of CM (Figure 13c) and SP2 (Figure 13e). SP2 is able to capture the general pattern of the observed anomalous higher relative humidity throughout the troposphere with a peak in the middle troposphere before high-rainfall events, especially in SP2_CL (Figure 13e), although it overestimates the anomalous high RH (Figure 13d). This high relative humidity explains why SP2 has a quicker transition to deep convection and more rainfall in the afternoon (Figure 7d). SP1 also improves the simulations of RH anomalies before high-rainfall events but still produces biases in the upper atmosphere (Figures 13f and 13g). Overall, SP2_CL best captures the pattern of anomalous high RH before and after high-rainfall events, although it somehow overestimates the moistening effect of convection after the high-rainfall events (Figures 13a and 13e). Also, SP2 shows stronger RH before and less gradual drying after high-rainfall

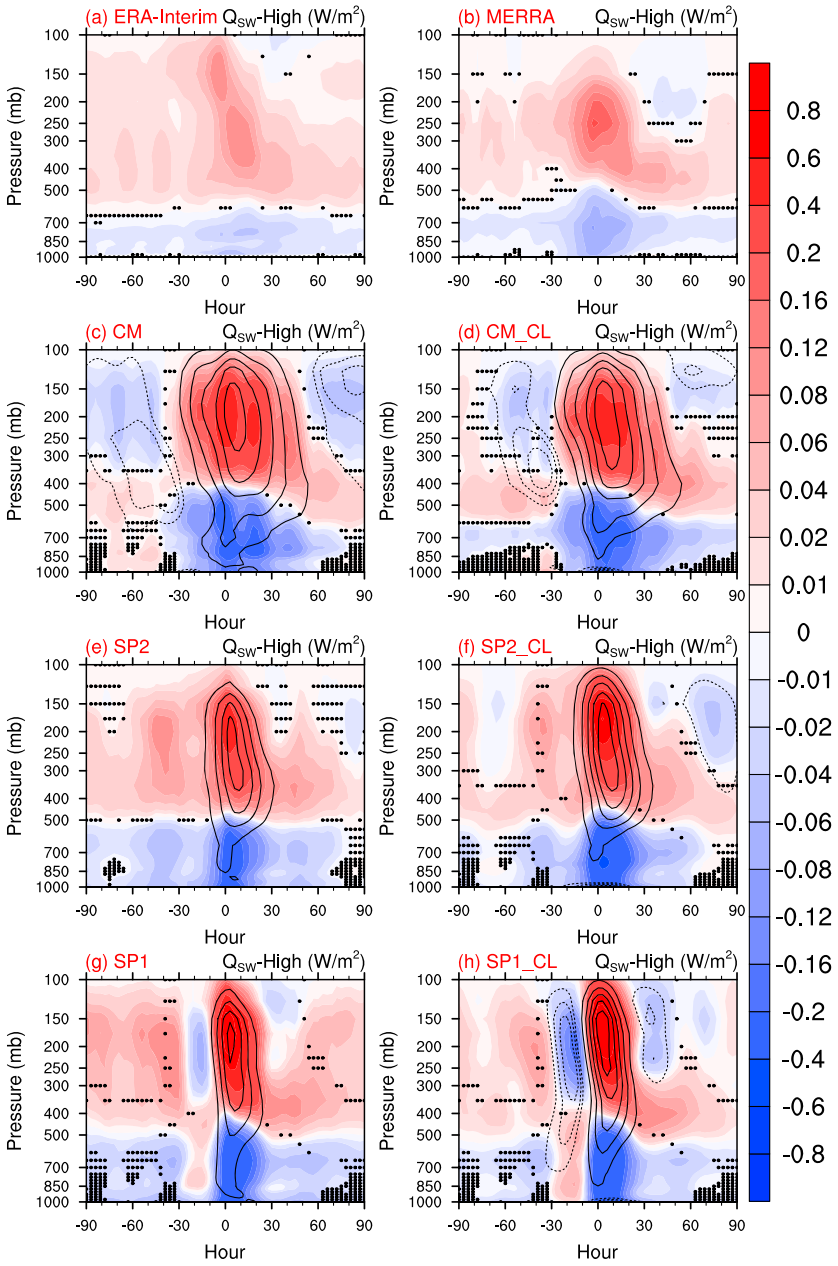

Figure 14. Same as Figure 13 but for shortwave heating anomalies (K/d). Overlaid black lines represent cloud fraction composites: dash lines represent negative anomalies with an interval of 0.01%, and solid lines represent positive anomalies with an interval of 0.05%.

events compared with the observations. The results for low-precipitation events almost mirror those for high-precipitation events shown here.

Figures 14 and 15 evaluate anomalous solar and longwave heating distributions before and after high-rainfall events, and cloud composites shown by black contours. Both reanalyses show a persistent negative solar anomaly (Figure 14a) in the lower troposphere and positive in the upper troposphere before and after high-precipitation events. Such patterns are consistent with influences of middle and upper tropospheric clouds that reflect solar radiation in the upper troposphere and reduce the solar radiation reaching the lower troposphere (contours in Figure 14). The middle tropospheric clouds also reduce upwelling longwave to the upper troposphere and increase downwelling longwave back to the lower troposphere (Figure 15). In the days before and after the high-rainfall events, CM and CM_CL simulate the opposite to that observed, i.e.,

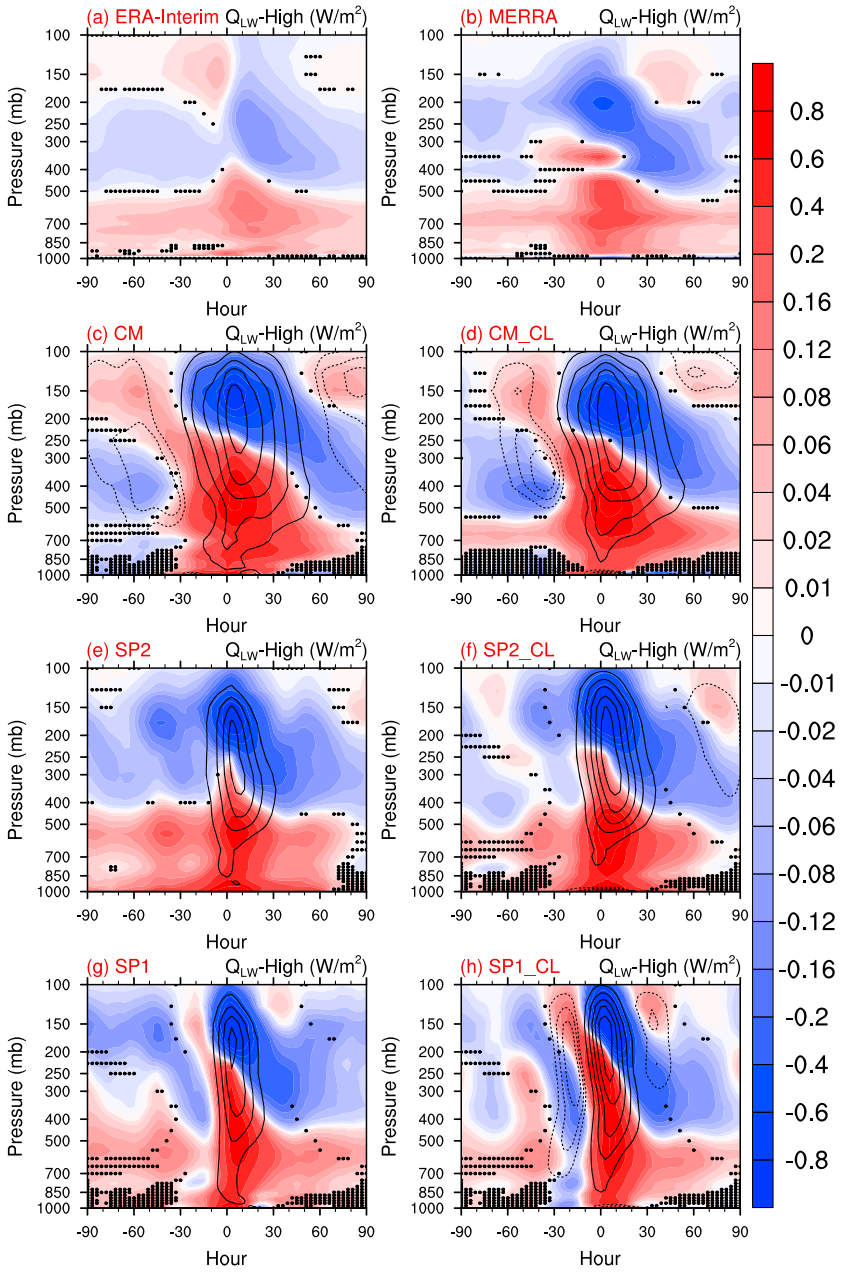

Figure 15. Same as Figure 14 but for longwave heating anomalies (K/d).

negative solar anomaly and positive longwave anomaly in the upper troposphere and anomalous solar warming and longwave cooling in the lower troposphere (Figures 14b, 14c, 15b, and 15c), opposite to that observed (Figures 14a and 15a). However, SP2 and SP2_CL both capture the general patterns of anomalous cloudiness and thus solar and longwave heating as observed (Figures 14d, 14e, 15d, and 15e). SP1 and SP1_CL produce opposite patterns during 10–30 h before high-rainfall events compared with observations (Figures 14f, 14g, 15f, and 15g).

In summary, observations show increased relative humidity prior to deep convection events. SP2 and SP2_CL appear to enable the models to capture this phenomenon. In contrast, the CM and CM_CL tend to have to a low bias in relative humidity and solar heating in the upper troposphere and too high solar heating in the middle to lower atmosphere before and after convection (Figures 13c, 13d, 14c, and 14d). SP1_CL also shows this bias but to a lesser degree.

4. Conclusions and Discussion

In this study, we conduct six numerical experiments to investigate the differences between rainfall over southern Amazonia simulated by CM, CM_CL, SP2, SP2_CL, SP1, and SP1_CL. Low biases of rainfall in current state-of-the-art climate models over southern Amazonia have been documented (e.g., Li et al., 2006; Yin et al., 2013). This paper explores how different treatments of convection, namely, the updated Zhang-McFarlane scheme in CM, SP and CLUBB, affect rainfall biases over Amazonia. Our results suggest that turbulence and shallow cloud schemes such as CLUBB that better simulate the transition from shallow-to-deep convection, or include more realistic representations of cloud and precipitation processes, aerosol effects, and convective dynamics such as SP, can improve the rainfall diurnal cycle and reduce the low-rainfall biases during the wet season. They also better represent the transition between the dry to wet seasons than does the traditional convective treatment in CM. The combination of both SP (especially with its aerosol treatment) and CLUBB (SP2_CL) produces not only the most realistic wet-season rainfall but also the observed relationships between convection and large-scale environmental conditions, and anomalous radiative heating. However, none of these convective treatments are able to reduce the dry bias during the dry season over Amazonia.

Observational studies have suggested that aerosols can invigorate and increase the lifetimes of deep convection over tropical continents (e.g., Chakraborty et al., 2016; Lin et al., 2006). However, assessing the physical and dynamical feedbacks involved in aerosol-cloud-precipitation interactions in climate models, such as entrainment and evaporative cooling, is quite difficult (e.g., Ackerman et al., 2004). Our simulations show that CM with two-moment cloud physics and aerosol effect in stratiform clouds only, as well as SP with one-moment cloud microphysics without aerosol effect, do not significantly reduce the dry bias. Only SP with two-moment cloud microphysics and the effect of aerosols in all cloud types (especially convective clouds) can significantly remove the dry bias in the wet season. These results suggest the importance of the cloud microphysics and aerosol effects on convective and all cloud types for adequately modeling rain rate over Amazonia. Similar results by Lim et al. (2014) comparing simulations over East Asia with and without cloud microphysics and aerosol effects in the ZM scheme also support our findings. Lim et al. (2014) noted that when cloud microphysics and aerosol effects are included in the ZM scheme, convection detrains more cloud water and ice mass, which increases precipitation from the stratiform clouds.

With CLUBB, low biases of humidity in the lower troposphere are significantly reduced. The resultant stronger lower tropospheric instability (Figure 10) with the increased MSE likely contributes to more rainfall and high clouds. SP2 makes the lower atmosphere more unstable with higher atmospheric temperatures and more moisture, further generating more deep convection and allowing the growth of more extreme convection. All the models except for CM_CL have dry biases and thus lack condensation and latent heating in the boundary layer.

In terms of the diurnal cycle, the superparameterization significantly increases deep convection and precipitation in the afternoon, but rainfall still peaks earlier than observed, while CLUBB exhibits delays in the afternoon peak time and more precipitation in the early morning. It also simulates an intermediate transition stage from shallow-to-deep convection and from deep-to-shallow convection, which helps the deep convection to grow and decay more gradually, thus delaying the peak time and increasing the period of precipitation events. SP increases, even overestimates, precipitation in the afternoon, but only delays the timing of the precipitation peak by around 2 h.

The reasons for the precipitation changes in implementing CLUBB and SP are investigated in terms of instability and moisture fields. The SP models generally produce more moist static energy (Figures 10d–10g), in part due to higher temperature (Figures 3a and 3b). The changes in mean precipitation amounts generally correspond to changes in the moist static energy fields, which reflect the fact that the change in atmospheric stability might be a primary reason for the changes in precipitation simulations.

In observations, relative humidity is increased prior to deep convection events. Only the SP2 verisons (SP2 and SP2_CL) can capture this phenomenon. Thus, SP2 appears to best simulate the transition to deep convection in the afternoon among the six model versions (Figure 7d). CM and CM_CL tend to underestimate precipitation and overestimate solar heating in the low atmosphere. Also, the cloud microphysics with aerosol treatment helps to improve the simulations significantly, especially the development of convection.

Recently, a unified formulation of large-scale GCMs and local-scale CRMs has been used in global atmosphere models (e.g., Arakawa & Konor, 2009; Arakawa & Wu, 2013; Arakawa et al., 2011). Comparison between conventional GCMs and Multiscale Modeling Frameworks becomes increasingly important in improving multiscale atmospheric modeling. The comparison between CM, CM_CL, SP2, SP2_CL, SP1, and SP1_CL presented here provides new evidence for how improvements in convection, microphysics, and aerosol-cloud parameterizations can help improve the precipitation in simulations over the southern Amazon region in the context of global models.

Acknowledgments
This work was supported by the DOE/FAPEAM/FAPESP GOAmazon project under grants DE-SC0011117. S. Ghan and L.R. Leung were supported by the U.S. Department of Energy, Office of Science, Regional and Global Climate Modeling program. Battelle Memorial Institute operates the Pacific Northwest National Laboratory for the DOE under contract DE-AC06-76RLO-1830. M. Wang was supported by the Jiangsu Province Specially appointed professorship grant, the One Thousand Young Talents Program, and by the National Natural Science Foundation of China (41575073 and 41621005). Jose Marengo was supported by FAPESP/DOE/FAPEAM GoAmazon grant 2013/50538-7. ERA-Interim data sets were retrieved via ECMWF Web API (https://software.ecmwf.int/wiki/display/WEBAPI/Access+ECMWF+Public+Datasets). MERRA and TRMM data sets were downloaded from Goddard Earth Sciences Data and Information Services Center (https://disc.sci.gsfc.nasa.gov). The model outputs are available upon request.

References

Ackerman, A. S., Kirkpatrick, M. P., Stevens, D. E., & Toon, O. B. (2004). The impact of humidity above stratiform clouds on indirect aerosol climate forcing. *Nature*, *432*(7020), 1014–1017.

Adler, R. F., Huffman, G. J., Chang, A., Ferraro, R., Xie, P.-P., Janowiak, J., … Bolvin, D. (2003). The version-2 global precipitation climatology project (GPCP) monthly precipitation analysis (1979–present). *Journal of Hydrometeorology*, *4*(6), 1147–1167.

Andreae, M. O., Rosenfeld, D., Artaxo, P., Costa, A., Frank, G., Longo, K., & Silva-Dias, M. (2004). Smoking rain clouds over the Amazon. *Science*, *303*(5662), 1337–1342.

Arakawa, A., & Konor, C. S. (2009). Unification of the anelastic and quasi-hydrostatic systems of equations. *Monthly Weather Review*, *137*(2), 710–726.

Arakawa, A., & Wu, C.-M. (2013). A unified representation of deep moist convection in numerical modeling of the atmosphere. Part I. *Journal of Atmospheric Science*, *70*(7), 1977–1992.

Arakawa, A., Jung, J.-H., & Wu, C.-M. (2011). Toward unification of the multiscale modeling of the atmosphere. *Atmos. Chem. Phys.*, *11*(8), 3731–3742.

Benedict, J. J., & Randall, D. A. (2009). Structure of the Madden–Julian oscillation in the superparameterized CAM. *Journal of Atmospheric Science*, *66*(11), 3277–3296.

Bogenschutz, P. A., Gettelman, A., Morrison, H., Larson, V. E., Craig, C., & Schanen, D. P. (2013). Higher-order turbulence closure and its impact on climate simulations in the Community Atmosphere Model. *Journal of Climatology*, *26*(23), 9655–9676.

Bretherton, C. S., & Park, S. (2009). A new moist turbulence parameterization in the Community Atmosphere Model. *Journal of Climatology*, *22*(12), 3422–3448.

Chakraborty, S., Fu, R., Massie, S. T., & Stephens, G. (2016). Relative influence of meteorological conditions and aerosols on the lifetime of mesoscale convective systems. *Proceedings of the National Academy of Sciences*, 201601935

Collins, W. D., Rasch, P. J., Boville, B. A., Hack, J. J., McCaa, J. R., Williamson, D. L., … Lin, S. (2004). Description of the NCAR Community Atmosphere Model (CAM 3.0) (NCAR Tech. Note NCAR/TN-464+ STR, 226).

Cox, P. M., Betts, R., Collins, M., Harris, P., Huntingford, C., & Jones, C. (2004). Amazonian forest dieback under climate-carbon cycle projections for the 21st century. *Theoretical and Applied Climatology*, *78*(1–3), 137–156.

Dai, A., Giorgi, F., & Trenberth, K. E. (1999). Observed and model-simulated diurnal cycles of precipitation over the contiguous United States. *Journal of Geophysical Research*, *104*(D6), 6377–6402.

Dee, D. P., Uppala, S. M., Simmons, A. J., Berrisford, P., Poli, P., Kobayashi, S., … Bauer, P. (2011). The ERA-Interim reanalysis: Configuration and performance of the data assimilation system. *Quarterly Journal of the Royal Meteorological Society*, *137*(656), 553–597.

DeMott, C. A., Stan, C., Randall, D. A., Kinter, J. L. III, & Khairoutdinov, M. (2011). The Asian monsoon in the superparameterized CCSM and its relationship to tropical wave activity. *Journal of Climatology*, *24*(19), 5134–5156.

Derbyshire, S., Beau, I., Bechtold, P., Grandpeix, J. Y., Piriou, J. M., Redelsperger, J. L., & Soares, P. (2004). Sensitivity of moist convection to environmental humidity. *Quarterly Journal of the Royal Meteorological Society*, *130*(604), 3055–3079.

Field, C. B., Behrenfeld, M. J., Randerson, J. T., & Falkowski, P. (1998). Primary production of the biosphere: Integrating terrestrial and oceanic components. *Science*, *281*(5374), 237–240.

Friedlingstein, P., Cox, P., Betts, R., Bopp, L., Von Bloh, W., Brovkin, V., … Fung, I. (2006). Climate-carbon cycle feedback analysis: Results from the C4MIP model intercomparison. *Journal of Climatology*, *19*(14), 3337–3353.

Friedlingstein, P., Andrew, R. M., Rogelj, J., Peters, G., Canadell, J. G., Knutti, R., … Van Vuuren, D. (2014). Persistent growth of CO_2 emissions and implications for reaching climate targets. *Nature Genetics*, *7*(10), 709–715.

Fu, R., Yin, L., Li, W., Arias, P. A., Dickinson, R. E., Huang, L., … Fisher, R. (2013). Increased dry-season length over southern Amazonia in recent decades and its implication for future climate projection. *Proceedings of the National Academy of Sciences*, *110*(45), 18110–18115.

Gent, P. R., Danabasoglu, G., Donner, L. J., Holland, M. M., Hunke, E. C., Jayne, S. R., … Vertenstein, M. (2011). The community climate system model version 4. *Journal of Climatology*, *24*(19), 4973–4991.

Gettelman, A., Morrison, H., & Ghan, S. J. (2008). A new two-moment bulk stratiform cloud microphysics scheme in the Community Atmosphere Model, version 3 (CAM3). Part II: Single-column and global results. *Journal of Climatology*, *21*(15), 3660–3679.

Golaz, J.-C., Larson, V. E., & Cotton, W. R. (2002). A PDF-based model for boundary layer clouds. Part I: Method and model description. *Journal of Atmospheric Science*, *59*(24), 3540–3551.

Grabowski, W. W. (2001). Coupling cloud processes with the large-scale dynamics using the cloud-resolving convection parameterization (CRCP). *Journal of Atmospheric Science*, *58*, 978–997.

Grabowski, W. W., & Moncrieff, M. (2004). Moisture–convection feedback in the tropics. *Quarterly Journal of the Royal Meteorological Society*, *130*(604), 3081–3104.

Gustafson, W. I. Jr., Berg, L. K., Easter, R. C., & Ghan, S. J. (2008). The explicit-cloud parameterized-pollutant hybrid approach for aerosol–cloud interactions in multiscale modeling framework models: Tracer transport results. *Environmental Research Letters*, *3*(2), 025005.

Holloway, C. E., & Neelin, J. D. (2009). Moisture vertical structure, column water vapor, and tropical deep convection. *Journal of Atmospheric Science*, *66*(6), 1665–1683.

Khairoutdinov, M. F., & Randall, D. A. (2001). A cloud resolving model as a cloud parameterization in the NCAR Community Climate System Model: Preliminary results. *Geophysical Research Letters*, *28*(18), 3617–3620.

Khairoutdinov, M. F., & Randall, D. A. (2003). Cloud resolving modeling of the ARM summer 1997 IOP: Model formulation, results, uncertainties, and sensitivities. *Journal of Atmospheric Science*, *60*(4), 607–625.

Khairoutdinov, M., Randall, D., & DeMott, C. (2005). Simulations of the atmospheric general circulation using a cloud-resolving model as a superparameterization of physical processes. *Journal of Atmospheric Science*, *62*(7), 2136–2154.

Khairoutdinov, M., DeMott, C., & Randall, D. (2008). Evaluation of the simulated interannual and subseasonal variability in an AMIP-style simulation using the CSU multiscale modeling framework. *Journal of Climatology*, *21*(3), 413–431.

Kooperman, G. J., Pritchard, M. S., & Somerville, R. C. (2013). Robustness and sensitivities of central US summer convection in the super-parameterized CAM: Multi-model intercomparison with a new regional EOF index. *Geophysical Research Letters*, *40*, 3287–3291. https://doi.org/10.1002/grl.50597

Kooperman, G. J., Pritchard, M. S., Burt, M. A., Branson, M. D., & Randall, D. A. (2016). Impacts of cloud superparameterization on projected daily rainfall intensity climate changes in multiple versions of the Community Earth System Model. *Journal of Advances in Modeling Earth Systems*, *8*, 1727–1750.

Koren, I., Kaufman, Y. J., Remer, L. A., & Martins, J. V. (2004). Measurement of the effect of Amazon smoke on inhibition of cloud formation. *Science*, *303*(5662), 1342–1345.

Koren, I., Martins, J. V., Remer, L. A., & Afargan, H. (2008). Smoke invigoration versus inhibition of clouds over the Amazon. *Science*, *321*(5891), 946–949.

Krishnamurthy, V., & Stan, C. (2015). Simulation of the South American climate by a coupled model with super-parameterized convection. *Climate Dynamics*, *44*(9–10), 2369–2382.

Kummerow, C., Simpson, J., Thiele, O., Barnes, W., Chang, A., Stocker, E., … Wentz, F. (2000). The status of the Tropical Rainfall Measuring Mission (TRMM) after two years in orbit. *Journal of Applied Meteorology*, *39*(12), 1965–1982.

Larson, V. E., & Golaz, J.-C. (2005). Using probability density functions to derive consistent closure relationships among higher-order moments. *Monthly Weather Review*, *133*(4), 1023–1042.

Larson, V. E., Schanen, D. P., Wang, M., Ovchinnikov, M., & Ghan, S. (2012). PDF parameterization of boundary layer clouds in models with horizontal grid spacings from 2 to 16 km. *Monthly Weather Review*, *140*(1), 285–306.

Li, C., Jia, X., Ling, J., Zhou, W., & Zhang, C. (2009). Sensitivity of MJO simulations to diabatic heating profiles. *Climate Dynamics*, *32*(2–3), 167–187.

Li, W., Fu, R., & Dickinson, R. E. (2006). Rainfall and its seasonality over the Amazon in the 21st century as assessed by the coupled models for the IPCC AR4. *Journal of Geophysical Research*, *111*, D02111. https://doi.org/10.1029/2005JD006355

Lim, K. S. S., Fan, J., Leung, L. R., Ma, P. L., Singh, B., Zhao, C., … Song, X. (2014). Investigation of aerosol indirect effects using a cumulus microphysics parameterization in a regional climate model. *Journal of Geophysical Research: Atmospheres*, *119*, 906–926. https://doi.org/10.1002/2013JD020958

Lin, J. C., Matsui, T., Pielke, R., & Kummerow, C. (2006). Effects of biomass-burning-derived aerosols on precipitation and clouds in the Amazon Basin: A satellite-based empirical study. *Journal of Geophysical Research*, *111*, D19204. https://doi.org/10.1029/2005JD006884

Ling, J., & Zhang, C. (2013). Diabatic heating profiles in recent global reanalyses. *Journal of Climatology*, *26*(10), 3307–3325.

Liu, X., Easter, R. C., Ghan, S. J., Zaveri, R., Rasch, P., Shi, X., … Vitt, F. (2012). Toward a minimal representation of aerosols in climate models: Description and evaluation in the Community Atmosphere Model CAM5. *Geoscientific Model Development*, *5*(3), 709.

Martin, S., Artaxo, P., Machado, L., Manzi, A., Souza, R., Schumacher, C., … Calheiros, A. (2016). The Green Ocean Amazon experiment (GoAmazon2014/5) observes pollution affecting gases, aerosols, clouds, and rainfall over the rain forest. *Bulletin of the American Meteorological Society*, *98*(5), 981–997.

McCrary, R. R., Randall, D. A., & Stan, C. (2014). Simulations of the West African monsoon with a superparameterized climate model. Part II: African easterly waves. *Journal of Climatology*, *27*(22), 8323–8341.

Mlawer, E. J., Taubman, S. J., Brown, P. D., Iacono, M. J., & Clough, S. A. (1997). Radiative transfer for inhomogeneous atmospheres: RRTM, a validated correlated-k model for the longwave. *Journal of Geophysical Research*, *102*(D14), 16663–16682.

Morrison, H., & Gettelman, A. (2008). A new two-moment bulk stratiform cloud microphysics scheme in the Community Atmosphere Model, version 3 (CAM3). Part I: Description and numerical tests. *Journal of Climatology*, *21*(15), 3642–3659.

Neale, R. B., Richter, J. H., & Jochum, M. (2008). The impact of convection on ENSO: From a delayed oscillator to a series of events. *Journal of Climatology*, *21*(22), 5904–5924.

Neale, R. B., Chen, C.-C., Gettelman, A., Lauritzen, P. H., Park, S., Williamson, D. L., … Lamarque, J.-F. (2010). Description of the NCAR Community Atmosphere Model (CAM 5.0) (NCAR Tech. Note NCAR/TN-486+ STR).

Park, S., & Bretherton, C. S. (2009). The University of Washington shallow convection and moist turbulence schemes and their impact on climate simulations with the Community Atmosphere Model. *Journal of Climatology*, *22*(12), 3449–3469.

Park, S., Bretherton, C. S., & Rasch, P. J. (2014). Integrating cloud processes in the Community Atmosphere Model, version 5. *Journal of Climatology*, *27*(18), 6821–6856.

Pritchard, M. S., Moncrieff, M. W., & Somerville, R. C. (2011). Orogenic propagating precipitation systems over the United States in a global climate model with embedded explicit convection. *Journal of Atmospheric Science*, *68*(8), 1821–1840.

Rienecker, M. M., Suarez, M. J., Gelaro, R., Todling, R., Bacmeister, J., Liu, E., … Kim, G.-K. (2011). MERRA: NASA's Modern-Era Retrospective Analysis for Research and Applications. *Journal of Climatology*, *24*(14), 3624–3648.

Sato, T., Miura, H., Satoh, M., Takayabu, Y. N., & Wang, Y. (2009). Diurnal cycle of precipitation in the tropics simulated in a global cloud-resolving model. *Journal of Climatology*, *22*(18), 4809–4826.

Song, X., Zhang, G. J., & Li, J.-L. (2012). Evaluation of microphysics parameterization for convective clouds in the NCAR Community Atmosphere Model CAM5. *Journal of Climatology*, *25*(24), 8568–8590.

Tao, W.-K., Chern, J.-D., Atlas, R., Randall, D., Khairoutdinov, M., Li, J.-L., … Peters-Lidard, C. (2009). A multiscale modeling system: Developments, applications, and critical issues. *Bulletin of the American Meteorological Society*, *90*(4), 515.

Vera, C., Silvestri, G., Liebmann, B., & González, P. (2006). Climate change scenarios for seasonal precipitation in South America from IPCC-AR4 models. *Geophysical Research Letters*, *33*, L13707. https://doi.org/10.1029/2006GL025759

Waite, M. L., & Khouider, B. (2010). The deepening of tropical convection by congestus preconditioning. *Journal of Atmospheric Science*, *67*(8), 2601–2615.

Wang, H., & Fu, R. (2002). Cross-equatorial flow and seasonal cycle of precipitation over South America. *Journal of Climatology*, *15*, 1591–1608.

Wang, M., Ghan, S., Easter, R., Ovchinnikov, M., Liu, X., Kassianov, E., … Schanen, D. (2011a). The multi-scale aerosol-climate model PNNL-MMF: Model description and evaluations. *Geoscientific Model Development*, *4*, 137–168.

Wang, M., Ghan, S., Ovchinnikov, M., Liu, X., Easter, R., Kassianov, E., … Morrison, H. (2011b). Aerosol indirect effects in a multi-scale aerosol-climate model PNNL-MMF. *Atmos. Chem. Phys.*, *11*(11), 5431.

Wang, M., Larson, V. E., Ghan, S., Ovchinnikov, M., Schanen, D. P., Xiao, H., … Guo, Z. (2015). A multiscale modeling framework model (superparameterized CAM5) with a higher-order turbulence closure: Model description and low-cloud simulations. *Journal of Advances in Modeling Earth Systems.*, *7*(2), 484–509.

Warner, T. T., Mapes, B. E., & Xu, M. (2003). Diurnal patterns of rainfall in northwestern South America. Part II: Model simulations. *Monthly Weather Review*, *131*(5), 813–829.

Wendisch, M., Pöschl, U., Andreae, M. O., Machado, L. A., Albrecht, R., Schlager, H., … Afchine, A. (2016). ACRIDICON–CHUVA campaign: Studying tropical deep convective clouds and precipitation over Amazonia using the new German research aircraft HALO. *Bulletin of the American Meteorological Society*, *97*(10), 1885–1908.

Yin, L., Fu, R., Shevliakova, E., & Dickinson, R. E. (2013). How well can CMIP5 simulate precipitation and its controlling processes over tropical South America? *Climate Dynamics*, *41*(11–12), 3127–3143.

Zhang, G. J., & McFarlane, N. A. (1995). Sensitivity of climate simulations to the parameterization of cumulus convection in the Canadian Climate Centre general circulation model. *Atmos. Ocean*, *33*(3), 407–446.

Zhang, K., Randel, W. J., & Fu, R. (2016). Relationships between outgoing longwave radiation and diabatic heating in reanalyses. *Climate Dynamics*, *1–19*, 2911–2929. https://doi.org/10.1007/s00382-016-3501-0

Zhuang, Y., Fu, R., Marengo, J., & Wang, H. (2017). Seasonal variation of shallow-to-deep convection transition and its link to the environmental conditions over the Central Amazon. *Journal of Geophysical Research: Atmospheres*, *122*, 2649–2666. https://doi.org/10.1002/2016JD025993